Indentation and penetration of a spherical elastic membrane filled with fluid

by

Amir Hosein Aboudzadeh Deris
B.Sc., Tehran Polytechnic, 2011

A Dissertation Submitted in Partial Fulfillment of the
Requirements for the Degree of

Master of Applied Science

in the Department of Mechanical Engineering

Indentation and penetration of a spherical elastic membrane filled with fluid

by

Amir Hosein Aboudzadeh Deris

B.Sc., Tehran Polytechnic, 2011

Supervisory Committee

_____

Dr. Ben Nadler, Supervisor

(Department of Mechanical Engineering)

_____

Dr. Henning Struchtrup, Departmental Member

(Department of Mechanical Engineering)

Supervisory Committee

Dr. Ben Nadler, Supervisor
(Department of Mechanical Engineering)

Dr. Henning Struchtrup, Departmental Member
(Department of Mechanical Engineering)

ABSTRACT

The applications of elastic membrane range from determining the mechanical properties of biological cells by indentation tests to predicting the deformed shape of a large commercial tent structure. In this work, direct membrane theory and a particular Varga strain energy function are used to model the indentation and puncturing of an isotropic spherical elastic membrane containing a fluid with a rigid indenter. The balance laws are applied to obtain the governing differential equations and numerical shooting method is used to solve them. Furthermore, a global mode of failure is established by computing the energy stored at the punctured membrane and this value determines a critical value for the energy of the membrane beyond which the punctured state of the membrane is energetically preferred. An additional mode of failure is identified in which the membrane loses local convexity requirements and it corresponds to the local loss of elastic behaviour of the membrane.

Contents

List of Tables

List of Figures

ACKNOWLEDGEMENTS

I would like to thank:

I believe I know the only cure, which is to make one's centre of life inside of one's self, not selfishly or excludingly, but with a kind of unassailable serenity-to decorate one's inner house so richly that one is content there, glad to welcome any one who wants to come and stay, but happy all the same in the hours when one is inevitably alone.

Edith Wharton

DEDICATION

Dedicated to my beloved family

Chapter 1

Introduction

Membranes are thin structures with plane stresses and the basic assumption in membrane theory is that the stress in the thickness direction is negligible. They have a variety of applications and their mechanical behaviour has been studied extensively in the literature for numerous problems. For example, membranes are used in large commercial tent structures that can cover large areas effectively and membrane theory as well as finite element analysis are used to study the deformation of membranes in this context. Other examples of membranes include protective gloves, condoms, biological cells and balloons that have applications such as angioplasty.

It should be noted that membranes do not have any bending stiffness and if they are subject to negative plane stresses they buckle in a phenomenon known as wrinkling. Different algorithms for treatment of wrinkling has been proposed in the literature. For instance, tension field theory and relaxed strain energy density functions are theories proposed by Dr. A. C. Pipkin, D. J. Steigmann and others to provide analysis for wrinkling [8], [9].

In continuum mechanics theory, cavitation is an interesting phenomenon in which a point maps into a finite curve which produces infinite stretch and not every strain energy function can model such a singularity. J. M. Ball [1] extensively studied a class of singular solutions for the equations of non-linear elastostatics containing a spherical hole at the centre of a ball of isotropic material subject to prescribed surface traction or displacement and he called this phenomenon cavitation. The existence of such solutions depends on the behaviour of the strain energy function at large strains and he proposed that any continuum mechanics theory that tries to model cavitation must make assumptions on the material behaviour for arbitrary large strains. He showed that at a critical boundary traction or displacement, the singular solution containing

cavity bifurcates from a trivial homogeneous solution which becomes unstable.

Studying cavitation for membranes dates back to the works of D. M. Haughton. In [2], he considered an incompressible, isotropic elastic membrane subjected to equibiaxial tension. He used several class of strain energy functions and in each case he proved that solutions containing cavity could not exist. In [3], he considered a thin disk made of Blatz-Ko compressible elastic material subjected to a uniform radial tension. He showed that solutions containing cavity exist as long as tension exceeds some critical value. Moreover, he used a membrane theory derived from three-dimensional theory of elasticity to show that cavitation is not possible for homogeneous, isotropic, compressible Varga strain energy function for the same problem.

D. J. Steigmann [4], used the direct theory of membranes to study cavitation and the qualitative behaviour of a two-dimensional version of the strain energy function given in [3] for Varga material. Plane axisymmetric deformations of a solid circular disk with prescribed boundary displacements were considered and it was shown that deformation containing a central hole is possible as long as the prescribed edge displacements exceeds a critical value. Furthermore, it was shown that equilibrium deformations with cavitation minimizes the energy in the class of plane axisymmetric deformations.

According to D. J. Steigmann [6], in real applications puncturing is probably an irreversible process and the use of elasticity theory in this problem can be rationalized by viewing the cavitation as the growth of a pre-existing hole with small radius. Moreover, C. O. Horgan and R. Abeyaratne [5] worked on a bifurcation plain strain problem for cylinders made of Blatz-Ko material and explained the problem in terms of the growth of a pre-existing micro-void. They prescribed the radial stretch for the outer surface of an isotropic compressible elastic cylinder and interestingly, they showed that the cavity in the center does not appear until the radial stretch at the boundary reaches to a critical value.

D. J. Steigmann in [6] considered the problem of puncturing an isotropic elastic membrane by a rigid indenter. According to this article, the puncturing induced by indenter is fundamentally different from cavitation induced by prescribing boundary data alone and puncturing is possible in membranes that can not sustain conventional cavitation. Moreover, a relaxed strain energy function was considered and the Legendre-Fenchel dual of the relaxed strain-energy was used to compute a complementary energy associated with the relaxed strain energy. The requirement for existence of the deformation gradient for a prescribed stress in this context was also

mentioned. This complementary energy was used to obtain a lower bound on the total stored energy that is strictly increasing function of the indenter displacement; thus, establishing the existence of a critical displacement beyond which the penetrated state of the membrane is energetically favourable. Moreover, some results were given for the Varga strain-energy function.

In [7], B. Nadler and D. J. Steigmann considered a sequence of axisymmetric equilibrium deformations of a flat circular membrane indented by a rigid cylindrical indenter. A strain energy function that can sustain both penetration and cavitation was developed which is an example of a class of energies discussed in [4]. Furthermore, it was shown that if the prescribed boundary radius exceeds a certain value, cavitated state in which the membrane is no longer in contact with the indenter and a central traction-free hole is formed is possible.

There are many articles in the literature that discuss the deformation of membranes in various problems and the following list provides a sample of those articles and it is not a complete list.

In [8], A. C. Pipkin showed that tension filed theory can be integrated with the ordinary theory of elastic membranes by using a suitable relaxed energy density function and consequently, no compressive stress appears in the solution of a membrane problem. Therefore, the strain energy function of the material in wrinkled regions can be substituted by a relaxed strain-energy function that satisfies all the required convexity conditions and ensures the non-negativity of the stresses. Furthermore, the necessary and sufficient conditions for Legendre-Hadamard inequality for isotropic membranes were derived in this paper. In [10], he also argued that in the theory of elastic membranes, the strain energy function is a function of deformation gradient which is a matrix with dimension 3×2 and due to objectivity, it should be a function of right Cauchy-Green deformation tensor. Material stability requires that the strain energy to be a quasiconvex function of the deformation gradient tensor. It is not easy to check the quasiconvexity property; however, if the strain energy is convex or polyconvex then it is quasiconvex and quasiconvexity implies rank-one convexity and these alternative conditions were investigated in this paper. Moreover, it is convenient to treat deformation gradient matrix as a 2×2 matrix rather than 3×2 matrix and in this article, he showed that by doing so, there is no loss of generality in the sense that strain energy function is convex with respect to 3×2 matrices if and only if it is convex with respect to 2×2 matrices.

W. W. Feng and P. Huang [11] studied the non-axisymmetric friction-less contact

of an inflated membrane which is initially flat with a fixed rigid indenter. Minimum potential energy principle was used to find the deformed configuration of the membrane and as an example, a square plane membrane with Mooney strain energy was considered

In [12], D. M. Haughton considered the loading of axisymmetric isotropic elastic membranes by incompressible fluid and he showed that the deformed shape can be determined by controlling the initial thickness of the membrane and a critical loading was observed in which the membrane goes through a very sudden change of shape.

X. Li and D. J. Steigmann in [13] considered a pressurized hemispherical isotropic elastic membrane subject to a concentrated force. A relaxed strain energy based on Ogden's incompressible three-term strain energy function was used to accommodate wrinkling. It was shown that the solution exists as long as the strain energy satisfies a certain growth condition which is satisfied by Ogden's strain energy function but fails for many other frequently used functions.

D. J. Steigmann used direct membrane theory in [14] to study bifurcation of a thin square elastic sheet to a rectangle at a critical value of the equibiaxial dead load. The stability requirements for homogeneous solutions of pure traction boundary-value problems were established. As an example, the strain energy function proposed in [7] was considered and it was shown that the solution is unstable if the square root of the determinant of right Cauchy-Green deformation tensor exceeds a certain value.

B. Nadler [15] considered the contact of a spherical elastic and isotropic membrane containing fluid with rigid parallel planes and used the relaxed strain energy function introduced in [8] to provide an analysis for wrinkling. Moreover, N. Kumar and A. DasGupta [16] considered the contact of an inflated spherical hyperelastic membrane with rigid parallel plates for different contact conditions. Isotropic Mooney-Rivlin strain energy function was used and certain results were established including the minimum inflation necessary to avoid wrinkling at any point in the membrane.

A. Libai and D. Givoli [17] analysed a non-linear axisymmetric hyperelastic membrane under pulling force. The governing differential equations in the tense and wrinkled regions were obtained and a numerical algorithm based on shooting method was used for solution. It was shown that the initial Gaussian curvature of the surface has a profound effect on the response of the material.

B. Nadler and T. Tang [18] considered large deformation in the form of adhesion and decohesion of a non-linear axisymmetric membrane with a rigid flat punch and they showed that a non-linear analysis provides a behaviour that is substantially

different than what linear theory predicts.

C. T. Nguyen, T. Vu-Khanh, P. I. Dolez and J. Lara [19] studied the puncturing of elastomer membranes with sharp indenters and they showed that the behaviour and mechanisms of puncture by conical indenters is quite different from those of sharp needles.

T. Sohail and B. Nadler [20] considered the indentation of an elastic, homogeneous and isotropic spherical membrane containing an incompressible fluid with a rigid conical indenter and they showed that the sharpness of the indenter effects the stress distribution in the membrane.

H. Andra, M. K. Warby and J. R. Whiteman in [23] discussed the inflation of an incompressible isotropic hyperelastic membrane into a rigid mould caused by pressure and the existence of the solution for various relaxed strain energy functions was investigated.

M. R. Begley and T. J. Mackin in [24] considered the indentation of a clamped circular membrane with a frictionless spherical indenter. Certain analytical and numerical results were established that can be used to extract mechanical properties of thin films for which the conventional uni-axial tension experiments are problematic.

S. P. Pearce, J. R. King and M. J. Holdsworth [25] used non-linear elasticity theory and different strain-energy functions to model large deformations caused by indentation of an axisymmetric elastic membrane by a rigid body. Physical application of such indentations include puncture of robber gloves by medical needles and stones embedding into rubber tyres.

However, there is very little information on the indentation and puncturing of spherical membranes in the literature and no article was found that considers this case specifically. The goal of this research is to consider the indentation and penetration of a spherical isotropic elastic membrane which contains a fluid by a rigid indenter. This work provides more insight in the penetration and possibility of cavitation for spherical membranes and it can possibly be extended to model real applications such as cell indentation or injection.

In Chapter 2, the problem is formulated and direct membrane theory is used to obtain governing ordinary differential equations. Moreover, strain energy function is introduced and a suitable strain energy function is formulated which is used to find the energy stored in the membrane at the punctured state. In addition, two failure criteria considered in this work are introduced in this Chapter. In Chapter 3, numerical algorithm used for the solution is explained. Initial inflation, approximation

of derivatives at problematic points and computation of volume are also explained in this Chapter. In Chapter 4, non-dimensional variables are introduced and numerical results are presented and interpreted. Furthermore, additional numerical results are given in appendix A. Finally in Chapter 5, the conclusions and recommendations of this research are presented. The list of symbols that are used frequently throughout this thesis is presented in Table 1.1.

Table 1.1: List of Symbols

Symbol	Definition
R	referential radius of membrane
r_0	inflated radius of the membrane
$\{\phi, \theta\}$	curvilinear coordinates in the reference configuration
$\mathbf{G}_\alpha$, $\mathbf{G}^\alpha$	covariant and contravariant basis in the reference configuration
$\mathbf{g}_\alpha$, $\mathbf{g}^\alpha$	covariant and contravariant basis in the deformed configuration
$G_{\alpha\beta}$, $G^{\alpha\beta}$	covariant and contravariant components of the referential metric tensor
$\{\mathbf{E}_R, \mathbf{E}_\phi, \mathbf{E}_\theta\}$	referential spherical basis
$\{\mathbf{e}_r, \mathbf{e}_\psi, \mathbf{e}_\theta\}$	spatial spherical basis
$\{\mathbf{i}, \mathbf{j}, \mathbf{k}\}$	spatial cylindrical basis
$\mathbf{F}$	deformation gradient tensor
$\mathbf{C}$	right Cauchy-Green deformation tensor
λ, μ	principal stretches
J	areal dilation
G	membrane shear modulus
I_1, I_2, I_3	principal scalar invariants of a tensor
$\mathbf{P}$	first Piola-Kirchhoff stress tensor
$\mathbf{T}$	Cauchy stress tensor
$\mathbf{I}$	identity tensor
$\mathbf{U}$	right stretch tensor
$\mathbf{Q}$	orthogonal transformation tensor
Grad, grad	referential and spatial gradient operator
Div, div	referential and spatial divergence operator
e	internal energy per referential area
Θ	temperature
ψ	Helmholtz free-energy per referential area
η	entropy per referential area
$\mathbf{q_0}$	referential heat flux vector
$\mathbf{b}$	body force per unit deformed area
$\mathbf{v}$	velocity
ρ	radius of the indenter
p_f	fluid pressure
p_c	contact pressure
u, h	horizontal and vertical positions in the deformed configuration
d	indenter displacement
E_p	energy stored at the punctured membrane
ϕ_{c_1}, ϕ_{c_2}	contacting angles with the indenter and support
λ_0, λ_π	polar stretches

Chapter 2

Problem Formulation

2.1 Deformation

In this thesis we consider the axisymmetric indentation and penetration of an isotropic elastic spherical membrane which is supported by a flat support and contains a fluid. The rigid indenter is a cylinder with radius ρ and has a hemispherical cap. Consider a membrane which in its reference configuration is a stress-free sphere of radius R. We denote this configuration by Γ where $\phi \in [0, \pi]$ and $\theta \in [0, 2\pi)$ are the convected curvilinear coordinates that are used for parametrizing its surface. The position of a material particle in this reference configuration can be expressed as

$$\mathbf{X} = R\mathbf{E}_R(\phi, \theta), \tag{2.1}$$

where $\{\mathbf{E}_R(\phi, \theta), \mathbf{E}_\phi(\phi, \theta), \mathbf{E}_\theta(\theta)\}$ is the right-handed orthonormal spherical basis for the reference configuration. The position in the axisymmetric deformed configuration of the membrane, which is denoted by γ, is expressed as

$$\mathbf{x} = r(\phi)\mathbf{e}_r(\psi, \theta), \tag{2.2}$$

where $\{\mathbf{e}_r(\psi, \theta), \mathbf{e}_\psi(\psi, \theta), \mathbf{e}_\theta(\theta)\}$ is the right-handed orthonormal spherical basis for the deformed configuration and r and ψ are functions of ϕ which are shown in Figure 2.1. The key ingredient in studying the deformation is the deformation gradient which determines the deformation in the neighbourhood of a material particle. In
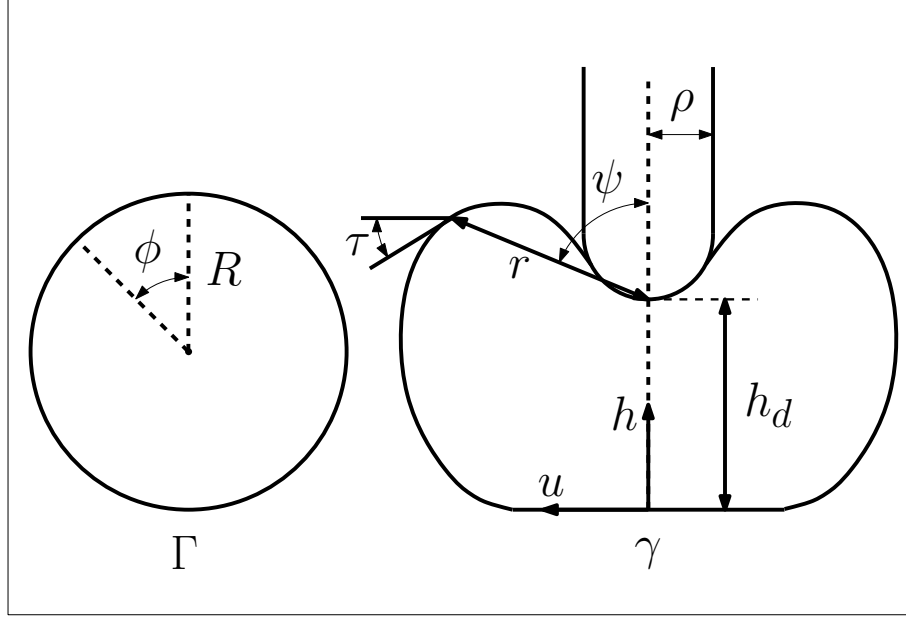
Figure 2.1: Reference (left figure) and deformed (right figure) configurations of the spherical membrane containing incompressible fluid.

general the deformation gradient can be computed in the following way

$$\mathbf{F} = \mathbf{g}_\alpha \otimes \mathbf{G}^\alpha, \tag{2.3}$$

where $\mathbf{g}_\alpha$ and $\mathbf{G}^\alpha$ are covariant basis in the deformed configuration and contravariant basis in the reference configuration, respectively. It should be noted that repeated index indicates summation convention and Greek indices take the values $\{1, 2\}$. To prove this equation, first we note that we use the convected curvilinear coordinates to parametrize the reference and deformed configuration and this set of curvilinear coordinates is denoted by $\{\theta^\alpha\}$. The differential of deformed position can be expressed as

$$\mathrm{d}\mathbf{x} = \mathbf{g}_\alpha \mathrm{d}\theta^\alpha, \tag{2.4}$$

where $\mathbf{g}_\alpha = \frac{\partial \mathbf{x}}{\partial \theta^\alpha}$. Similarly, the differential of the reference position can be expressed as

$$\mathrm{d}\mathbf{X} = \mathbf{G}_\alpha \mathrm{d}\theta^\alpha, \tag{2.5}$$

where $\mathbf{G}_\alpha = \frac{\partial \mathbf{X}}{\partial \theta^\alpha}$. By taking dot product of both sides of (2.5) by $\mathbf{G}^\beta$ and noting that $\mathbf{G}_\alpha \cdot \mathbf{G}^\beta = \delta_\alpha^\beta$ we have

$$\mathrm{d}\theta^\alpha = \mathrm{d}\mathbf{X} \cdot \mathbf{G}^\alpha. \tag{2.6}$$

By substituting (2.6) into (2.4) and using tensor product rule, we have

$$d\mathbf{x} = (\mathbf{g}_\alpha \otimes \mathbf{G}^\alpha)d\mathbf{X}. \tag{2.7}$$

Therefore by definition, the deformation gradient has the form shown in (2.3).

In our problem, the set of convected curvilinear coordinates are $\{\phi, \theta\}$ and in order to compute the deformation gradient from (2.3), we need to compute the derivatives of the spherical basis vectors with respect to this set of curvilinear coordinates. To find these derivatives, we can write the $\mathbf{e}_r$ and $\mathbf{e}_\psi$ as

$$\mathbf{e}_r(\psi, \theta) = \sin\psi \mathbf{i}(\theta) + \cos\psi \mathbf{k}, \tag{2.8}$$

$$\mathbf{e}_\psi(\psi, \theta) = \cos\psi \mathbf{i}(\theta) - \sin\psi \mathbf{k}, \tag{2.9}$$

$$\mathbf{e}_\theta(\theta) = \mathbf{j}(\theta), \tag{2.10}$$

where $\{\mathbf{e}_r, \mathbf{e}_\psi, \mathbf{e}_\theta\}$ is the spherical basis and $\{\mathbf{i}, \mathbf{j}, \mathbf{k}\}$ is the set of cylindrical basis in the deformed configuration, as shown in figure (2.2). By using the well known result
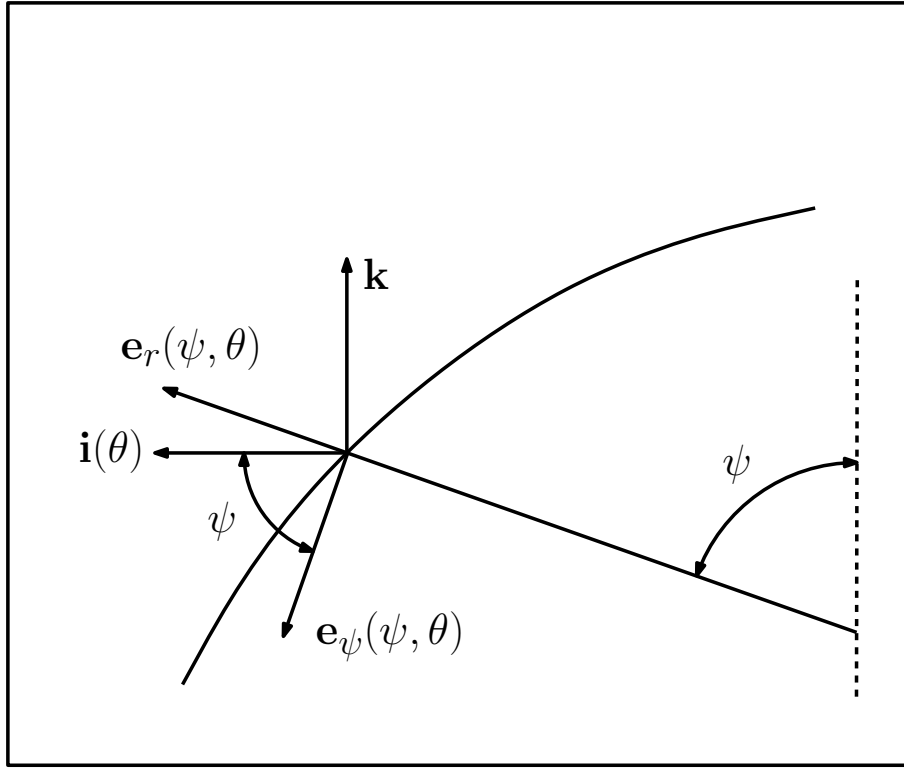
Figure 2.2: Spherical and cylindrical basis at a given point where $\mathbf{j} = \mathbf{k} \times \mathbf{i}$ and $\mathbf{e}_\theta = \mathbf{e}_r \times \mathbf{e}_\psi$

that $\frac{d\mathbf{i}}{d\theta} = \mathbf{j}$, we take the derivative of (2.8) with respect to ψ and θ and we have

$$\frac{\partial \mathbf{e}_r}{\partial \psi} = \cos \psi \mathbf{i} - \sin \psi \mathbf{k}, \tag{2.11}$$

$$\frac{\partial \mathbf{e}_r}{\partial \theta} = \sin \psi \mathbf{j} = \sin \psi \mathbf{e}_\theta. \tag{2.12}$$

By looking at Figure 2.2, it is clear that the right hand side of (2.11) is equal to $\mathbf{e}_\psi$; therefore, we have

$$\frac{\partial \mathbf{e}_r}{\partial \psi} = \mathbf{e}_\psi. \tag{2.13}$$

Now we can compute the covariant and contravariant basis to find the deformation gradient. By taking the derivative of (2.2) with respect to ϕ and θ and by using (2.12) and (2.13), we have

$$\mathbf{g}_1 = \mathbf{g}_\phi = \frac{\partial \mathbf{x}}{\partial \phi} = r'\mathbf{e}_r + r\psi'\mathbf{e}_\psi, \tag{2.14}$$

$$\mathbf{g}_2 = \mathbf{g}_\theta = \frac{\partial \mathbf{x}}{\partial \theta} = r \sin \psi \mathbf{e}_\theta, \tag{2.15}$$

where $()' = \frac{\partial ()}{\partial \phi}$. Furthermore, by taking the derivative of (2.1) with respect to ϕ and θ and by using the result of (2.12) and (2.13) for the reference configuration, we have

$$\mathbf{G}_1 = \mathbf{G}_\phi = \frac{\partial \mathbf{X}}{\partial \phi} = R\frac{\partial \mathbf{E}_R}{\partial \phi} = R\mathbf{E}_\phi, \tag{2.16}$$

$$\mathbf{G}_2 = \mathbf{G}_\theta = \frac{\partial \mathbf{X}}{\partial \theta} = R\frac{\partial \mathbf{E}_R}{\partial \theta} = R \sin \phi \mathbf{E}_\theta. \tag{2.17}$$

For using equation (2.3) we need to compute the contravariant basis in the reference configuration; therefore, first we construct the covariant metric tensor. The covariant components of the metric tensor in the reference configuration are computed in the following way

$$G_{\alpha\beta} = \mathbf{G}_\alpha \cdot \mathbf{G}_\beta, \tag{2.18}$$

where $G_{\alpha\beta}$ are the covariant metric tensor in the reference configuration. By substituting (2.16) and (2.17) into (2.18) we have

$$G_{11} = \mathbf{G}_1 \cdot \mathbf{G}_1 = R^2, \tag{2.19}$$

$$G_{22} = \mathbf{G}_2 \cdot \mathbf{G}_2 = R^2 \sin^2 \phi, \tag{2.20}$$

$$G_{12} = G_{21} = \mathbf{G}_1 \cdot \mathbf{G}_2 = 0. \tag{2.21}$$

Hence the covariant metric tensor for the reference configuration is

$$(G_{ij}) = \begin{pmatrix} R^2 & 0 \\ 0 & R^2 \sin^2 \phi \end{pmatrix}. \tag{2.22}$$

For computing the contravariant metric tensor, since by definition we have $\mathbf{G}_\alpha \cdot \mathbf{G}^\beta = \delta_\alpha^\beta$; therefore

$$\delta_\beta^\alpha = \mathbf{G}^\alpha \cdot \mathbf{G}_\beta = (G^{\alpha\gamma} \mathbf{G}_\gamma) \cdot \mathbf{G}_\beta = G^{\alpha\gamma} G_{\gamma\beta}, \tag{2.23}$$

which shows that contravariant metric tensor is the inverse of the covariant metric tensor. Therefore, by using (2.22) we have

$$(G^{\alpha\beta}) = (G_{\alpha\beta})^{-1} = \begin{pmatrix} R^2 & 0 \\ 0 & R^2 \sin^2 \phi \end{pmatrix}^{-1} = \begin{pmatrix} \frac{1}{R^2} & 0 \\ 0 & \frac{1}{R^2 \sin^2 \phi} \end{pmatrix}. \tag{2.24}$$

Since it is a well known result [21] that $\mathbf{G}^\alpha = G^{\alpha\beta} \mathbf{G}_\beta$, by using (2.16), (2.17) and (2.24) we can compute the contravariant basis vectors of the reference configuration in the following way

$$\mathbf{G}^1 = \mathbf{G}^\phi = G^{11} \mathbf{G}_1 + G^{12} \mathbf{G}_2 = \frac{1}{R^2} R \mathbf{E}_\phi = \frac{\mathbf{E}_\phi}{R}, \tag{2.25}$$

$$\mathbf{G}^2 = \mathbf{G}^\theta = G^{21} \mathbf{G}_1 + G^{22} \mathbf{G}_2 = \frac{1}{R^2 \sin^2 \phi} R \sin \phi \mathbf{E}_\theta = \frac{\mathbf{E}_\theta}{R \sin \phi}. \tag{2.26}$$

Finally, we can compute the deformation gradient by substituting (2.25), (2.26), (2.14) and (2.15) into (2.3)

$$\mathbf{F} = \mathbf{g}_1 \otimes \mathbf{G}^1 + \mathbf{g}_2 \otimes \mathbf{G}^2 = \frac{1}{R}(r' \mathbf{e}_r + r\psi' \mathbf{e}_\psi) \otimes \mathbf{E}_\phi + \frac{r \sin \psi}{R \sin \phi} \mathbf{e}_\theta \otimes \mathbf{E}_\theta. \tag{2.27}$$

In general, once a basis is chosen, the deformation gradient which is a 2nd order linear transformation (2nd order tensor), can be written as

$$F = F_{ij} \mathbf{e}_i \otimes \mathbf{E}_j, \tag{2.28}$$

where $\mathbf{e}_i$ and $\mathbf{E}_j$ are the basis of the deformed and reference configuration, respectively. By, comparing this to (2.27), it turns out that the basis of the deformed configuration is $\{\mathbf{e}_r, \mathbf{e}_\theta, \mathbf{e}_\psi\}$ and the basis of reference configuration is $\{\mathbf{E}_\phi, \mathbf{E}_\theta\}$; therefore, the dimension of the deformation gradient is 3×2. This is the result of the particular

choice of basis. Furthermore, the right Cauchy-Green deformation gradient which is a symmetric tensor, is defined by

$$\mathbf{C} = \mathbf{F}^{\mathrm{T}}\mathbf{F}, \tag{2.29}$$

where $\mathbf{C}$ is the right Cauchy-Green deformation gradient tensor and $\mathbf{F}^{\mathrm{T}}$ means transpose of $\mathbf{F}$. By using the eigenvectors of $\mathbf{C}$ as basis, we can write $\mathbf{C}$ as a diagonal matrix in principal basis (spectral representation)

$$\mathbf{C} = \lambda^2 \mathbf{L} \otimes \mathbf{L} + \mu^2 \mathbf{M} \otimes \mathbf{M}, \tag{2.30}$$

where λ and μ are principal stretches and they are always non-negative. Moreover, $\mathbf{L}$ and $\mathbf{M}$ are orthonormal principal strain axes on the reference configuration. By definition, the deformation gradient maps vectors from tangent plane of the reference configuration to the tangent plane of the deformed configuration; therefore, we can write

$$\mathbf{FL} = \lambda\mathbf{l}, \tag{2.31}$$

$$\mathbf{FM} = \mu\mathbf{m}, \tag{2.32}$$

where $\mathbf{L}$ and $\mathbf{M}$ by deformation gradient are mapped into unit vectors $\mathbf{l}$ and $\mathbf{m}$, respectively. We can prove that since $\mathbf{L}$ and $\mathbf{M}$ are orthonormal, $\mathbf{l}$ and $\mathbf{m}$ are also orthonormal. To prove this statement, we have

$$\mathbf{l} \cdot \mathbf{m} = \frac{\mathbf{FL}}{\lambda} \cdot \frac{\mathbf{FM}}{\mu} = \frac{1}{\lambda\mu}\mathbf{L} \cdot \mathbf{F}^{\mathbf{T}}\mathbf{FM} = \frac{1}{\lambda\mu}\mathbf{L} \cdot \mathbf{CM} = \frac{\mu}{\lambda}\mathbf{L} \cdot \mathbf{M} = 0, \tag{2.33}$$

where we have used (2.31), (2.32), (2.30) and property of dot product. This result shows that $\mathbf{F}$ preserves the angle between orthogonal eigenvectors of $\mathbf{C}$.

As stated in [6], now we can write the deformation gradient in the following way

$$\mathbf{F} = \mathbf{FI} = \mathbf{F}(\mathbf{L} \otimes \mathbf{L} + \mathbf{M} \otimes \mathbf{M}) = \mathbf{FL} \otimes \mathbf{L} + \mathbf{FM} \otimes \mathbf{M}, \tag{2.34}$$

where $\mathbf{I}$ is the referential identity tensor and we have used a property of tensor product. By using (2.31) and (2.32) we have:

$$\mathbf{F} = \lambda\mathbf{l} \otimes \mathbf{L} + \mu\mathbf{m} \otimes \mathbf{M}. \tag{2.35}$$

By comparing (2.35) to (2.27), we conclude that

$$\lambda = \frac{\sqrt{(r')^2 + (r\psi')^2}}{R}, \tag{2.36}$$

$$\mathbf{l} = \frac{r'\mathbf{e}_r + r\psi'\mathbf{e}_\psi}{\lambda R}, \tag{2.37}$$

$$\mathbf{L} = \mathbf{E}_\phi, \tag{2.38}$$

$$\mu = \frac{r\sin\psi}{R\sin\phi}, \tag{2.39}$$

$$\mathbf{m} = \mathbf{e}_\theta, \tag{2.40}$$

$$\mathbf{M} = \mathbf{E}_\theta. \tag{2.41}$$

To get a better understanding of the meaning of λ and μ, we can look at the geometry of the problem. By looking at Figure 2.3, we can write
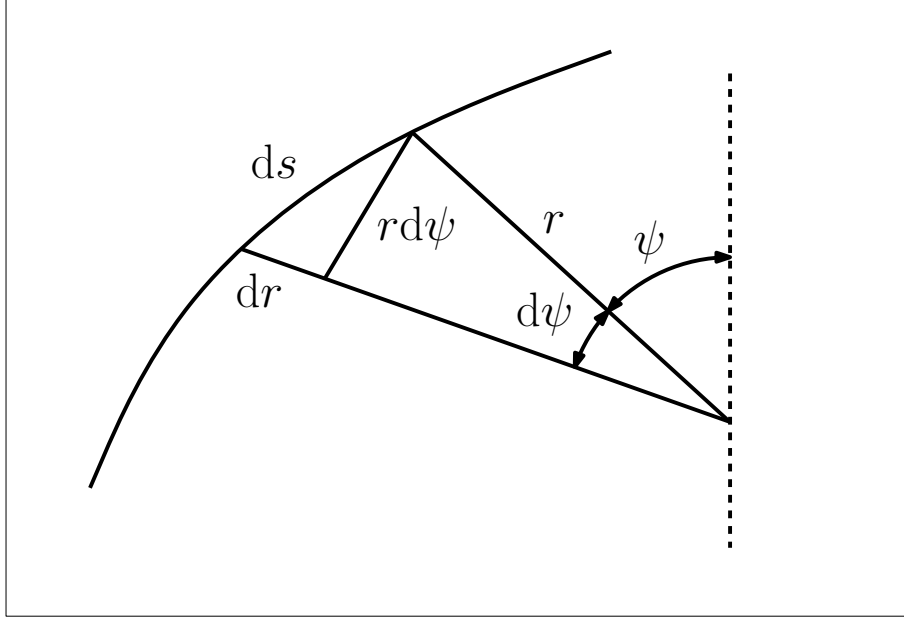
Figure 2.3: arc length in azimuthal direction for deformed configuration

$$ds = \sqrt{dr^2 + (rd\psi)^2} = \sqrt{(r')^2 + (r\psi')^2}d\phi, \tag{2.42}$$

where we have used the fact that r and ψ are functions of ϕ. On the other hand, it is clear that the corresponding arclength in the meridian direction in the reference

configuration is $\mathrm{d}S = R\mathrm{d}\phi$, therefore

$$\frac{\mathrm{d}s}{\mathrm{d}S} = \frac{\sqrt{(r')^2 + (r\psi')^2}}{R}, \tag{2.43}$$

which is the same as (2.36). Therefore, λ measures the ratio of the arclength in the azimuthal direction. Furthermore, by looking at Figure 2.4 we can write the ratio of arclength in circumferential direction as
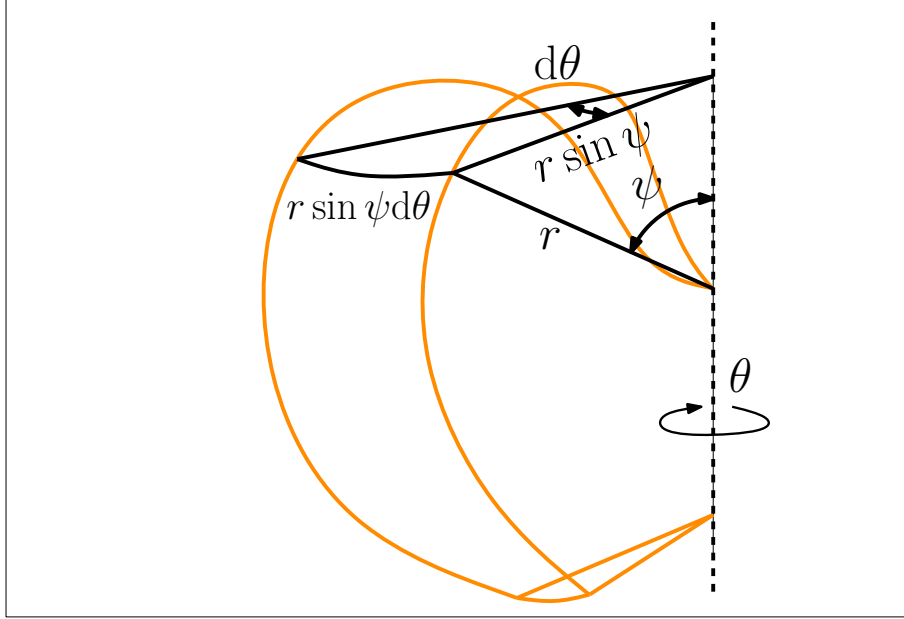
Figure 2.4: arc length in circumferential direction for deformed configuration

$$\frac{\mathrm{d}s}{\mathrm{d}S} = \frac{r\sin\psi\mathrm{d}\theta}{R\sin\phi\mathrm{d}\theta} = \frac{r\sin\psi}{R\sin\phi}, \tag{2.44}$$

which is similar to equation (2.39) so μ measures the ratio of the arclength in the circumferential direction.

The areal dilation is computed as

$$J = \sqrt{\det \mathbf{C}} = \lambda\mu, \tag{2.45}$$

where we have used (2.30). J represents the ratio of the area of an infinitesimal element in the deformed configuration to the area of its corresponding image in the reference configuration.

The outward normals to the tangent plane of the reference and deformed config-

uration are defined by

$$\mathbf{N} = \mathbf{L} \times \mathbf{M}, \tag{2.46}$$

$$\mathbf{n} = \mathbf{l} \times \mathbf{m}. \tag{2.47}$$

For finding the governing ordinary differential equations for r and ψ, we find the components of $\mathbf{l}$ in $\mathbf{e}_r$ and $\mathbf{e}_\psi$ directions. By looking at Figure 2.5 we have
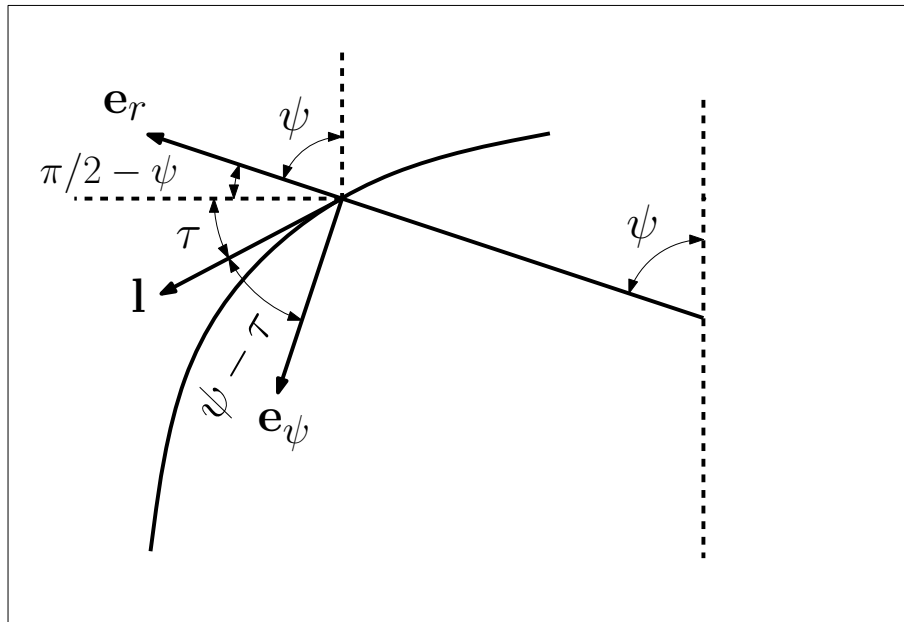
Figure 2.5: tangent vector $\mathbf{l}$ and its horizontal angle τ

$$\mathbf{l} = \sin{(\psi - \tau)}\mathbf{e}_r + \cos{(\psi - \tau)}\mathbf{e}_\psi, \tag{2.48}$$

where τ is the horizontal angle of $\mathbf{l}$. By equating this equation to (2.37) we get

$$r' = \lambda R \sin{(\psi - \tau)}, \tag{2.49}$$

$$r\psi' = \lambda R \cos{(\psi - \tau)}. \tag{2.50}$$

2.2 Strain Energy Function

According to second law of thermodynamics, the change of entropy is always greater than or equal to the rate of entropy input. The formulation for this section is given

in [27]. The Clausius-Duhem form of the second law of thermodynamics is given as

$$\mathbf{P} \cdot \dot{\mathbf{F}} - \dot{e} + \Theta\dot{\eta} - \frac{1}{\Theta}\mathbf{q_0}.\mathrm{Grad}\Theta \geq 0, \tag{2.51}$$

where $\mathbf{P}$ is the first Piola-Kirchhoff stress tensor, e is the internal energy density function per unit reference volume (area for membranes), Θ is the absolute temperature, η is the entropy density function per unit reference volume (area for membranes), $\mathbf{q_0}$ is the referential heat flux vector, Grad is the referential gradient and over dot indicates material time derivative. Moreover, the heat conduction inequality which is also known as Fourier inequality indicates that heat flows from warmer to colder region of a body

$$-\frac{1}{\Theta}\mathbf{q_0} \cdot \mathrm{Grad}\Theta \geq 0. \tag{2.52}$$

Considering inequalities (2.51) and (2.52), a stronger form of the second law of thermodynamics can be deduced which is known as Clausius-Planck inequality

$$\dot{s}_{gen} = \mathbf{P} \cdot \dot{\mathbf{F}} - \dot{e} + \Theta\dot{\eta} \geq 0, \tag{2.53}$$

where $\dot{s}_{gen}$ is the rate of local entropy production. Furthermore, the Helmholtz free-energy function per unit reference volume (area for membranes) is defined as

$$\Psi = e - \Theta\eta. \tag{2.54}$$

By using Legendre transformation, the Clausius-Planck inequality can be written as

$$\dot{s}_{gen} = \mathbf{P} \cdot \dot{\mathbf{F}} - \dot{\Psi} - \eta\dot{\Theta} \geq 0. \tag{2.55}$$

In this work, we consider a purely mechanical system and thermal effects are ignored; i.e., Θ and η are neglected. In this case, the Clausius-Planck inequality is reduced to

$$\mathbf{P} \cdot \dot{\mathbf{F}} - \dot{\Psi} \geq 0. \tag{2.56}$$

A hyperelastic material posses a Helmholtz free-energy function Ψ which is only function of deformation gradient $\Psi = \Psi(\mathbf{F})$ and in this case the Helmholtz free-energy function is referred to as strain-energy function [1].

---

[1]which is generally defined per unit reference volume and in the case of membranes, it is defined per unit reference area.

We also consider a homogeneous material in which the distribution of internal constituents are uniform and Ψ does not depend on the position of material points explicitly.

For a perfectly elastic material, $\dot{s}_{gen} = 0$ and inequality (2.56) becomes an equation which by using the fact that $\dot{\Psi} = \frac{\partial \Psi}{\partial \mathbf{F}} \cdot \dot{\mathbf{F}}$, will result in

$$(\mathbf{P} - \frac{\partial \Psi}{\partial \mathbf{F}}) \cdot \dot{\mathbf{F}} = 0. \tag{2.57}$$

Since the above equation must hold for all deformation rates $\dot{\mathbf{F}}$, we conclude the following equation that relates the first Piola-Kirchhoff stress tensor to the strain energy function

$$\mathbf{P} = \frac{\partial \Psi}{\partial \mathbf{F}}. \tag{2.58}$$

If the reference configuration is stress free, it is also required that

$$\Psi = \Psi(\mathbf{I}) = 0 \tag{2.59}$$

Moreover, certain growth conditions must also be satisfied by the strain energy function. These growth conditions indicate that $\Psi \to +\infty$ if $J = \det(\mathbf{F}) \to +\infty$ or $J = \det(\mathbf{F}) \to 0^+$.

Objectivity indicates that the stored energy can not change under superposed rigid body motion

$$\Psi(\mathbf{F}) = \Psi(\mathbf{Q}\mathbf{F}), \tag{2.60}$$

which holds for all $\mathbf{F}$ for which $\det(\mathbf{F}) > 0$ and for all orthogonal tensors $\mathbf{Q}$. By using polar decomposition theorem, we get

$$\Psi(\mathbf{F}) = \Psi(\mathbf{U}) = \Psi(\mathbf{C}), \tag{2.61}$$

where $\mathbf{U}$ is the right stretch tensor and it is related to the right Cauchy-Green deformation tensor

$$\mathbf{C} = \mathbf{U}^2. \tag{2.62}$$

Additionally, if the material is assumed to be isotropic, it means that the stored energy will not change if the reference configuration is subject to all rigid body motions before

the deformation. The result of isotropy is

$$\Psi(\mathbf{F}) = \Psi(\mathbf{FQ}^{\mathrm{T}}), \tag{2.63}$$

which holds for every orthogonal tensor $\mathbf{Q}$. It is interesting to note that (2.60) must hold for all materials and it is a physical requirement, while (2.63) only holds for isotropic materials. Considering the relation (2.61), the isotropy requirement implies that

$$\Psi(\mathbf{C}) = \Psi(\mathbf{QF}^{\mathrm{T}}\mathbf{FQ}^{\mathrm{T}}) = \Psi(\mathbf{QCQ}^{\mathrm{T}}). \tag{2.64}$$

Considering (2.64), the representation theorem for isotropic functions implies that Ψ must be a function of principal invariants of $\mathbf{C}$ for this equation to hold for all orthogonal tensors. Reference [29] contains the proof of this theorem. Therefore, we have

$$\Psi = \Psi\left(I_1(\mathbf{C}), I_2(\mathbf{C}), I_3(\mathbf{C})\right), \tag{2.65}$$

where $I_1(\mathbf{C})$, $I_2(\mathbf{C})$ and $I_3(\mathbf{C})$ are principal invariants of $\mathbf{C}$ which are defined as

$$I_1(\mathbf{C}) = \mathrm{tr}(\mathbf{C}) = \lambda_1^2 + \lambda_2^2 + \lambda_3^2, \tag{2.66}$$

$$I_2(\mathbf{C}) = \frac{1}{2}[(\mathrm{tr}\mathbf{C})^2 - \mathrm{tr}(\mathbf{C}^2)] = \lambda_1^2\lambda_2^2 + \lambda_2^2\lambda_3^2 + \lambda_3^2\lambda_1^2, \tag{2.67}$$

$$I_3(\mathbf{C}) = \det(\mathbf{C}) = \lambda_1^2\lambda_2^2\lambda_3^2, \tag{2.68}$$

where λ_i^2, $i \in \{1, 2, 3\}$ are the eigenvalues of $\mathbf{C}$. Since there is a one-to-one relationship between the invariants and the eigenvalues, we can conclude that

$$\Psi = \Psi(\lambda_1, \lambda_2, \lambda_3). \tag{2.69}$$

It is common in the literature to denote the Helmholtz free-energy function per unit reference volume (area for membranes) as w and call it strain energy function [28]. Therefore, for simplicity from now on we adopt this notation

$$w = w(\lambda_1, \lambda_2, \lambda_3). \tag{2.70}$$

Since we are using the direct theory of membranes, the material is a two-dimensional surface and we have

$$w = w(\lambda, \mu). \tag{2.71}$$

In this section, we try to find an strain energy function that is suitable for our problem. We seek a strain energy function that when λ or μ approach infinity, the total energy stored in the membrane stays finite. Since $u = r \sin \psi$ from (2.39) the hoop stretch can be written as

$$\mu = \frac{u}{R \sin \phi}, \tag{2.72}$$

as $\phi \to 0$, $u \to \rho$; therefore, $\mu \to \infty$ which shows that in the penetrated state of the membrane, the hoop stretch becomes infinity at $\phi = 0$.

The suitable strain energy function must satisfy some properties that are mentioned in [7] and we review them here.

According to [8], the Legendre-Hadamard inequality which implies rank-one convexity of strain energy is equivalent to the non-negativity of the second variation $\delta^2 W$ with respect to rank-one deformation gradient $\mathbf{a} \otimes \mathbf{b}$ where $W = W(\mathbf{F})$ is the strain energy function of a hyperelastic membrane and $\mathbf{a}$ and $\mathbf{b}$ are two vectors. By taking derivatives, for this condition we have

$$[W_{\mathbf{FF}}(\mathbf{a} \otimes \mathbf{b})] \cdot (\mathbf{a} \otimes \mathbf{b}) \geq 0, \tag{2.73}$$

where

$$W_{\mathbf{FF}} = \frac{\partial^2 W(\mathbf{F})}{\partial \mathbf{F}^2}. \tag{2.74}$$

The necessary and sufficient conditions for Legendre-Hadamard inequality for isotropic membranes are obtained in [8] and they are

$$w_\lambda \geq 0, \quad w_\mu \geq 0, \quad w_{\lambda\lambda} \geq 0, \quad w_{\mu\mu} \geq 0, \quad a \geq 0, \tag{2.75}$$

also

$$(w_{\lambda\lambda} w_{\mu\mu})^{1/2} - w_{\lambda\mu} \geq b - a, \quad (w_{\lambda\lambda} w_{\mu\mu})^{1/2} + w_{\lambda\mu} \geq -b - a, \tag{2.76}$$

where

$$a = \frac{\lambda w_\lambda - \mu w_\mu}{\lambda^2 - \mu^2} \quad \text{and} \quad b = \frac{\mu w_\lambda - \lambda w_\mu}{\lambda^2 - \mu^2}. \tag{2.77}$$

In this thesis, we use a particular Varga strain energy function. According to [3], the general three-dimensional compressible Varga strain energy function is defined as

$$w(\lambda_1, \lambda_2, \lambda_3) = 2G \left(\lambda_1 + \lambda_2 + \lambda_3 + g(\lambda_1 \lambda_2 \lambda_3)\right), \tag{2.78}$$

where $g()$ is a general function, G is the shear modulus and λ_i for $i \in \{1, 2, 3\}$ are

the principal stretches. The strain energy function used in this work is similar to (2.78) but it is for a purely two-dimensional surface. This strain energy function is introduced in [7] and it has the following form

$$w(\lambda, \mu) = 2G[I + F(J)], \tag{2.79}$$

where I and J are suitable two-dimensional invariants of the right Cauchy-Green deformation tensor defined as

$$J = \sqrt{\det \mathbf{C}} = \lambda\mu, \quad I = \sqrt{\operatorname{tr}\mathbf{C} + 2J} = \lambda + \mu, \tag{2.80}$$

and $F(J)$ is a function whose properties will be specified.

With (2.79), w_λ, w_μ, $w_{\lambda\lambda}$, $w_{\mu\mu}$, $w_{\lambda\mu}$ and a are computed as

$$w_\lambda = 2G(1 + F'\mu), \tag{2.81}$$
$$w_\mu = 2G(1 + F'\lambda), \tag{2.82}$$
$$w_{\lambda\lambda} = 2G(F''\mu^2), \tag{2.83}$$
$$w_{\mu\mu} = 2G(F''\lambda^2), \tag{2.84}$$
$$w_{\lambda\mu} = 2G(F''\lambda\mu + F'), \tag{2.85}$$
$$a = \frac{2G}{\lambda + \mu}, \tag{2.86}$$

According to (2.86) since λ and μ are always non-negative, a always satisfies $(2.75)_5$; furthermore, comparing (2.83) and (2.84) to $(2.75)_{3,4}$, we conclude that

$$F''(J) \geq 0, \tag{2.87}$$

where $F'' = \frac{d^2F}{dJ^2}$. Moreover, inequalities in (2.76) simplifies to

$$\frac{2}{\lambda + \mu} \geq 0, \quad 2F''\lambda\mu \geq 0. \tag{2.88}$$

Obviously, both of these inequalities are satisfied since λ and μ are always non-negative and also according to (2.87), $F'' \geq 0$.

As discussed in [8] and [7], the local convexity inequality

$$\mathbf{A} \cdot W_{\mathbf{FF}}[\mathbf{A}] \geq 0, \tag{2.89}$$

is stronger than (2.73) where $\mathbf{A}$ is any second order tensor which maps from tangent plane of reference configuration to tangent plane of deformed configuration. This condition is the requirement of the convexity and since convexity implies rank-one convexity, this condition is stronger than (2.73). Necessary and sufficient conditions for this inequality are mentioned in [7] and [8] and consist of inequalities (2.75) as well as the following

$$w_{\lambda\lambda}w_{\mu\mu} - w_{\lambda\mu}^2 \geq 0, \quad a \geq |b|. \tag{2.90}$$

It can be deduced [7] that the inequality $a \geq |b|$ is equivalent to $a + b \geq 0$ and $a - b \geq 0$. By using (2.77), we find expressions for $a - b$ and $a + b$

$$a - b = \frac{w_\lambda + w_\mu}{\lambda + \mu} \geq 0, \tag{2.91}$$

$$a + b = \frac{w_\lambda - w_\mu}{\lambda - \mu}. \geq 0 \tag{2.92}$$

By using inequality $(2.75)_{1,2}$ and noting the fact that stretches are always positive, we conclude that (2.91) is always satisfied. Furthermore, by using equations (2.83), (2.84) and (2.85) we can simplify $(2.90)_1$ and (2.92) to the following requirements

$$-4G^2 F'(F' + 2JF'') \geq 0, \tag{2.93}$$

$$F' \leq 0. \tag{2.94}$$

By using (2.94) into (2.93) we can simplify these requirements to this form

$$F' + 2JF'' \geq 0, \tag{2.95}$$

$$F' \leq 0, \tag{2.96}$$

For finding $F(J)$, we need to consider the punctured state of the membrane where part of the membrane is in contact with the cylindrical part of the indenter. Since the contact with the indenter is assumed to be frictionless, it is proved in the Section 2.6 that the stress w_λ vanishes in the part of the membrane which is in contact with the cylindrical part of the indenter after penetration occurs; therefore, from (2.81)

$$w_\lambda = 2G(1 + F'\mu) = 0 \implies F' = -\mu^{-1}. \tag{2.97}$$

Therefore (2.96) is strictly satisfied. We can assume that $F''(J) > 0$ for all $J > 0$ and according to implicit function theorem, (2.97) gives a unique J for each μ in this

region; therefore, we can write

$$J = \hat{J}(\mu), \tag{2.98}$$

where $\hat{J}(\mu)$ is that explicit function. By differentiating (2.97) with respect to μ and using chain rule we have

$$\frac{\partial F'}{\partial \mu} = \frac{\partial F'}{\partial J}\frac{\partial \hat{J}}{\partial \mu} = \mu^{-2}. \tag{2.99}$$

From (2.87) and using the fact that μ is always positive, (2.99) yields

$$\hat{J}' > 0, \tag{2.100}$$

which means J is strictly increasing in the contacting part of the membrane with the cylindrical part of the indenter at the penetrated state. Furthermore, we can assume $\hat{J}(1) = 1$. Moreover, as $\phi \to 0$, $\mu \to \infty$ and for satisfying (2.97) we can assume that F has an stationary point at $J = J_0$ such that $J \to J_0$ as $\mu \to \infty$ and therefore $F' \to 0$. From (2.100) and since we assumed $\hat{J}(1) = 1$, we conclude that

$$J_0 > 1. \tag{2.101}$$

Since the dilation J is only function of μ in this region, we can compute λ in the following way

$$\lambda = v(\mu) = \frac{\hat{J}(\mu)}{\mu}, \tag{2.102}$$

where $v(\mu)$ is called the natural width under uniaxial stress which represents the stretch in λ direction when only stress in the circumferential direction is non zero. By substituting (2.97) into (2.82) and using (2.102), we have

$$f(\mu) = w(v(\mu), \mu) = 2G\left(1 - \frac{v(\mu)}{\mu}\right) = 2G\left(1 - \frac{\hat{J}(\mu)}{\mu^2}\right), \tag{2.103}$$

where f is the stress in the circumferential direction (hoop stress) which is only function of μ in this region. We can assume $\mu > 1$ in this region and we conclude that $f(\mu) > 0$. By setting $f(1) = 0$, then for satisfying $(2.75)_4$ the sufficient condition is $f'(\mu) > 0$ for all $\mu > 0$. By taking the derivative of (2.103) with respect to μ and after simplifying, we have

$$\frac{\hat{J}'(\mu)}{\hat{J}(\mu)} < \frac{2}{\mu}, \quad \mu > 0. \tag{2.104}$$

By integrating the above equation we get

$$\int_1^\mu \frac{\hat{J}'(x)}{\hat{J}(x)}dx < \ln \mu^2, \quad \mu > 1, \tag{2.105}$$

$$\int_\mu^1 \frac{\hat{J}'(x)}{\hat{J}(x)}dx < -\ln \mu^2, \quad 0 < \mu < 1. \tag{2.106}$$

Simplifying the above equation and setting $\hat{J}(1) = 1$, yields

$$\ln\left(\hat{J}(\mu)\right) < \ln \mu^2, \quad \mu > 1, \tag{2.107}$$

$$\ln\left(\hat{J}(\mu)\right) > \ln \mu^2, \quad 0 < \mu < 1. \tag{2.108}$$

Since the logarithmic function is monotonically increasing, we conclude that

$$\hat{J}(\mu) < \mu^2, \quad \mu > 1, \tag{2.109}$$

$$\hat{J}(\mu) > \mu^2, \quad 0 < \mu < 1. \tag{2.110}$$

If we impose $\hat{J}(0) = 0$, a sufficient condition to satisfy the above requirements is to have $\hat{J}''(\mu) < 0$ for $\mu > 0$.

As proposed in [7], a simple function that satisfies all the previous requirements is

$$\hat{J}(\mu) = \frac{J_0\mu}{J_0 - 1 + \mu}. \tag{2.111}$$

By taking derivative of the above equation and checking equation (2.104), we see that this requirement is satisfied. By finding μ from (2.111) and substitute into (2.97) we get

$$F'(J) = \frac{1}{J_0 - 1}\left(1 - \frac{J_0}{J}\right). \tag{2.112}$$

By checking the above equation for $J = 1$, we get $F'(1) = -1$ which from (2.81) and (2.82) we see that the reference configuration is stress free as required. Also, we see that (2.96) is satisfied as long as $J < J_0$ which we use later in section Section 2.7 as an additional failure criteria beside energy criteria to identify the point of failure in the indentation process. By taking the derivative of (2.112), we find

$$F''(J) = \frac{J_0}{J_0 - 1}\left(\frac{1}{J^2}\right). \tag{2.113}$$

The above equation satisfies (2.87) since $J_0 > 1$ as discussed before. Furthermore, we can compute the expression in (2.95) to get

$$F' + 2JF'' = \frac{1}{J_0 - 1}\left(1 + \frac{J_0}{J}\right), \tag{2.114}$$

which satisfies the requirement in (2.95). For finding $F(J)$, we integrate (2.112) and we obtain

$$F(J) - F(1) = \int_{x=1}^{x=J} \frac{1}{J_0 - 1}\left(1 - \frac{J_0}{x}\right) dx. \tag{2.115}$$

From (2.79), in order to have no energy in the reference configuration, we set $F(1) = -2$ and finally by integrating the above equation we have the following form for $F(J)$

$$F(J) = \frac{1}{J_0 - 1}(1 + J - 2J_0 - J_0 \ln J). \tag{2.116}$$

By obtaining $F(J)$, we have the following expressions for the energy and stresses which are obtained from (2.79) to (2.85)

$$w(\lambda, \mu) = 2G\left(\lambda + \mu + \frac{1}{J_0 - 1}(1 + \lambda\mu - 2J_0 - J_0 \ln(\lambda\mu))\right), \tag{2.117}$$

$$w_\lambda = 2G\left(1 + \frac{1}{J_0 - 1}(\mu - \frac{J_0}{\lambda})\right), \tag{2.118}$$

$$w_\mu = 2G\left(1 + \frac{1}{J_0 - 1}(\lambda - \frac{J_0}{\mu})\right), \tag{2.119}$$

$$w_{\lambda\lambda} = \frac{2GJ_0}{(J_0 - 1)\lambda^2}, \tag{2.120}$$

$$w_{\mu\mu} = \frac{2GJ_0}{(J_0 - 1)\mu^2}, \tag{2.121}$$

$$w_{\lambda\mu} = \frac{2G}{J_0 - 1}. \tag{2.122}$$

2.3   Equilibrium

2.3.1   Membrane

The spatial statement of the balance of linear momentum is given as

$$\text{div}\mathbf{T} + \rho\mathbf{b} = \rho\frac{D\mathbf{v}}{Dt}, \tag{2.123}$$

where div is the spatial divergence operator, $\mathbf{T}$ is the Cauchy stress tensor, ρ is the mass per unit deformed area, $\mathbf{b}$ is the body force per unit mass, $\mathbf{v}$ is the velocity and $\mathrm{D}()/\mathrm{D}t$ indicates material time derivative. For finding the referential statement of balance of linear momentum, we multiply the above equation by areal dilation J and we have

$$J\mathrm{div}\mathbf{T} + \rho J\mathbf{b} = \rho J\frac{\mathrm{D}\mathbf{v}}{\mathrm{D}t}. \tag{2.124}$$

Since we are interested in equilibrium configurations, $\frac{\mathrm{D}\mathbf{v}}{\mathrm{D}t} = \mathbf{0}$. Furthermore, by introducing $\mathbf{f} = \rho\mathbf{b}$ we can rewrite the above equation

$$J\mathrm{div}\mathbf{T} + J\mathbf{f} = \mathbf{0}, \tag{2.125}$$

where $\mathbf{f}$ is the body force per unit deformed area. There is a well known result in continuum mechanics that indicates that $J\mathrm{div}\mathbf{T} = \mathrm{Div}\mathbf{P}$ where $\mathbf{P}$ is the first Piola-Kirchhoff stress tensor and Div is the divergence operator in the reference configuration. By using this result we have

$$\mathrm{Div}\mathbf{P} + J\mathbf{f} = \mathbf{0}. \tag{2.126}$$

For computing $\mathbf{P}$, we use equation (2.58). For this purpose, we take the differential of (2.35) and we have

$$d\mathbf{F} = d\lambda\mathbf{l} \otimes \mathbf{L} + \lambda d\mathbf{l} \otimes \mathbf{L} + d\mu\mathbf{m} \otimes \mathbf{M} + \mu d\mathbf{m} \otimes \mathbf{M}. \tag{2.127}$$

By operating both sides on $\mathbf{L}$ and using the fact that $\mathbf{L}$ and $\mathbf{M}$ are orthonormal, we have

$$d\mathbf{F}\mathbf{L} = d\lambda\mathbf{l} + \lambda d\mathbf{l}. \tag{2.128}$$

By taking the dot product of above equation with $\mathbf{l}$ we get

$$(d\mathbf{F}\mathbf{L}) \cdot \mathbf{l} = d\lambda + \lambda d\mathbf{l} \cdot \mathbf{l}. \tag{2.129}$$

However, since $\mathbf{l} \cdot \mathbf{l} = 1$, we have $d\mathbf{l} \cdot \mathbf{l} = 0$; therefore

$$d\lambda = (d\mathbf{F}\mathbf{L}) \cdot \mathbf{l}. \tag{2.130}$$

By using tensor algebra [26] we can write the above equation in the following form

$$d\lambda = (\mathbf{l} \otimes \mathbf{L}) \cdot d\mathbf{F}. \tag{2.131}$$

Similarly, we have

$$d\mu = (\mathbf{m} \otimes \mathbf{M}) \cdot d\mathbf{F}. \tag{2.132}$$

Furthermore, the differential of strain energy function (2.71) is

$$dw = w_\lambda d\lambda + w_\mu d\mu, \tag{2.133}$$

where $w_\lambda = \frac{\partial w}{\partial \lambda}$, $w_\mu = \frac{\partial w}{\partial \mu}$ and $w(\lambda, \mu)$ is the strain energy function which is discussed in section Section 2.2. Finally, by substituting (2.131) and (2.132) into (2.133) we can compute the first Piola-Kirchhoff stress tensor

$$\mathbf{P} = w_\lambda \mathbf{l} \otimes \mathbf{L} + w_\mu \mathbf{m} \otimes \mathbf{M}. \tag{2.134}$$

In order to compute the Div$\mathbf{P}$, first we find a general relation to compute the referential Grad$\mathbf{A} = \frac{\partial \mathbf{A}}{\partial \mathbf{X}}$ where $\mathbf{A}$ is a tensor. We have

$$d\mathbf{A} = \frac{\partial \mathbf{A}}{\partial \theta_\alpha} d\theta^\alpha, \tag{2.135}$$

where $\{\theta^\alpha\}$ are the curvilinear coordinates for the reference configuration. By substituting (2.6) into equation (2.135) we have

$$d\mathbf{A} = (\frac{\partial \mathbf{A}}{\partial \theta_\alpha} \otimes \mathbf{G}^\alpha) d\mathbf{X}, \tag{2.136}$$

which means

$$\text{Grad}\mathbf{A} = \frac{\partial \mathbf{A}}{\partial \theta_\alpha} \otimes \mathbf{G}^\alpha. \tag{2.137}$$

Now we can use (2.137) to compute the referential gradient of $\mathbf{P}$. As stated before, the curvilinear coordinates are $\{\theta, \phi\}$; therefore

$$\text{Grad}\mathbf{P} = \frac{\partial \mathbf{P}}{\partial \theta} \otimes \mathbf{G}^\theta + \frac{\partial \mathbf{P}}{\partial \phi} \otimes \mathbf{G}^\phi. \tag{2.138}$$

We use the following well known results in the spherical coordinate system in order to compute the required derivatives

$$\frac{\partial \mathbf{E}_\phi}{\partial \theta} = \cos \phi \mathbf{E}_\theta, \tag{2.139}$$

$$\frac{\partial \mathbf{e}_\theta}{\partial \theta} = -\mathbf{i}, \tag{2.140}$$

$$\frac{\partial \mathbf{E}_\phi}{\partial \phi} = -\mathbf{E}_r, \tag{2.141}$$

where $\mathbf{i}$ is shown in Figure 2.2. By taking the derivatives of (2.134) with respect to θ and ϕ we have

$$\frac{\partial \mathbf{P}}{\partial \theta} = w_\lambda \frac{\partial \mathbf{l}}{\partial \theta} \otimes \mathbf{E}_\phi + w_\lambda \mathbf{l} \otimes \frac{\partial \mathbf{E}_\phi}{\partial \theta} + w_\mu \frac{\partial \mathbf{e}_\theta}{\partial \theta} \otimes \mathbf{E}_\theta + w_\mu \mathbf{e}_\theta \otimes \frac{\partial \mathbf{E}_\theta}{\partial \theta}, \tag{2.142}$$

where we have used the fact that since the problem is axisymmetric, $\frac{\partial w_\lambda}{\partial \theta} = \frac{\partial w_\mu}{\partial \theta} = 0$. Furthermore, by substituting (2.139) and (2.140) into the above equation we get

$$\frac{\partial \mathbf{P}}{\partial \theta} = w_\lambda \frac{\partial \mathbf{l}}{\partial \theta} \otimes \mathbf{E}_\phi + w_\lambda \cos \phi \mathbf{l} \otimes \mathbf{E}_\theta - w_\mu \mathbf{i} \otimes \mathbf{E}_\theta - w_\mu \mathbf{e}_\theta \otimes \mathbf{i}_R, \tag{2.143}$$

where $\mathbf{i}_R$ is the radial cylindrical basis in the reference configuration. Also, we compute $\frac{\partial \mathbf{P}}{\partial \phi}$ in the following way

$$\frac{\partial \mathbf{P}}{\partial \phi} = w'_\mu \mathbf{e}_\theta \otimes \mathbf{E}_\theta + w'_\lambda \mathbf{l} \otimes \mathbf{L} + w_\lambda \mathbf{l}' \otimes \mathbf{L} + w_\lambda \mathbf{l} \otimes \mathbf{L}', \tag{2.144}$$

where $()' = \frac{\partial ()}{\partial \phi}$ and by using equation (2.38) and (2.141) we obtain

$$\frac{\partial \mathbf{P}}{\partial \phi} = w'_\mu \mathbf{e}_\theta \otimes \mathbf{E}_\theta + w'_\lambda \mathbf{l} \otimes \mathbf{E}_\phi + w_\lambda \mathbf{l}' \otimes \mathbf{E}_\phi - w_\lambda \mathbf{l} \otimes \mathbf{E}_r. \tag{2.145}$$

Now we can use (2.25), (2.26), (2.143), (2.145) and (2.138) to compute the referential gradient of $\mathbf{P}$

$$\begin{aligned}
\text{Grad}\mathbf{P} = {} & \frac{1}{R \sin \phi} (w_\lambda \frac{\partial \mathbf{l}}{\partial \theta} \otimes \mathbf{E}_\phi \otimes \mathbf{E}_\theta + w_\lambda \cos \phi \mathbf{l} \otimes \mathbf{E}_\theta \otimes \mathbf{E}_\theta - w_\mu \mathbf{i} \otimes \mathbf{E}_\theta \otimes \mathbf{E}_\theta \\
& - w_\mu \mathbf{e}_\theta \otimes \mathbf{i}_R \otimes \mathbf{E}_\theta) + \frac{1}{R} (w'_\mu \mathbf{e}_\theta \otimes \mathbf{E}_\theta \otimes \mathbf{E}_\phi + w'_\lambda \mathbf{l} \otimes \mathbf{E}_\phi \otimes \mathbf{E}_\phi + w_\lambda \mathbf{l}' \otimes \mathbf{E}_\phi \otimes \mathbf{E}_\phi \\
& - w_\lambda \mathbf{l} \otimes \mathbf{E}_r \otimes \mathbf{E}_\phi).
\end{aligned} \tag{2.146}$$

As it can be seen, since $\mathbf{P}$ is a second order tensor, its gradient is a third order tensor. By definition, $\mathrm{Div}\mathbf{P} = \mathrm{tr}(\mathrm{Grad}\mathbf{P})$ and the trace of a general third order tensor by definition is computed as

$$\mathrm{tr}(A_{ijk}\mathbf{u_i} \otimes \mathbf{u_j} \otimes \mathbf{u_k}) = A_{ijk}(\mathbf{u_j} \cdot \mathbf{u_k})\mathbf{u_i}, \tag{2.147}$$

where $\mathbf{u_i}, \mathbf{u_j}$ and $\mathbf{u_k}$ are orthonormal basis vectors. Since the basis vectors are orthonormal, we have the following relations

$$\mathbf{E}_\phi \cdot \mathbf{E}_\theta = \mathbf{i}_R \cdot \mathbf{E}_\theta = \mathbf{E_r} \cdot \mathbf{E}_\phi = 0. \tag{2.148}$$

By using (2.148), (2.147) and (2.146) we have

$$\mathrm{Div}\mathbf{P} = \frac{1}{R\sin\phi}(w_\lambda\cos\phi\mathbf{l} - w_\mu\mathbf{i}) + \frac{1}{R}(w'_\lambda\mathbf{l} + w_\lambda\mathbf{l}'). \tag{2.149}$$

2.3.2 Fluid

Constitutive

Since the fluid can deform the membrane easily, we assume that the indenter can not compress the fluid; therefore, the fluid behaves like an incompressible material. Also, for simplicity we assume that the fluid is non-viscous and as it is mentioned in many Continuum Mechanics reference books [22], the stress in an incompressible inviscid fluid is given by

$$\mathbf{T}_f = -p_f\mathbf{I}, \tag{2.150}$$

where $\mathbf{T}_f$ is the Cauchy stress in the fluid and p_f is the fluid pressure.

Equilibrium For The Fluid

The traction that fluid exerts on the membrane is equal to

$$\mathbf{f_f} = p_f\mathbf{n}, \tag{2.151}$$

where $\mathbf{f_f}$ is the fluid traction exerted on the membrane and $\mathbf{n}$ is the normal to the membrane, as shown in Figure 2.6. By using the spatial balance of linear momentum
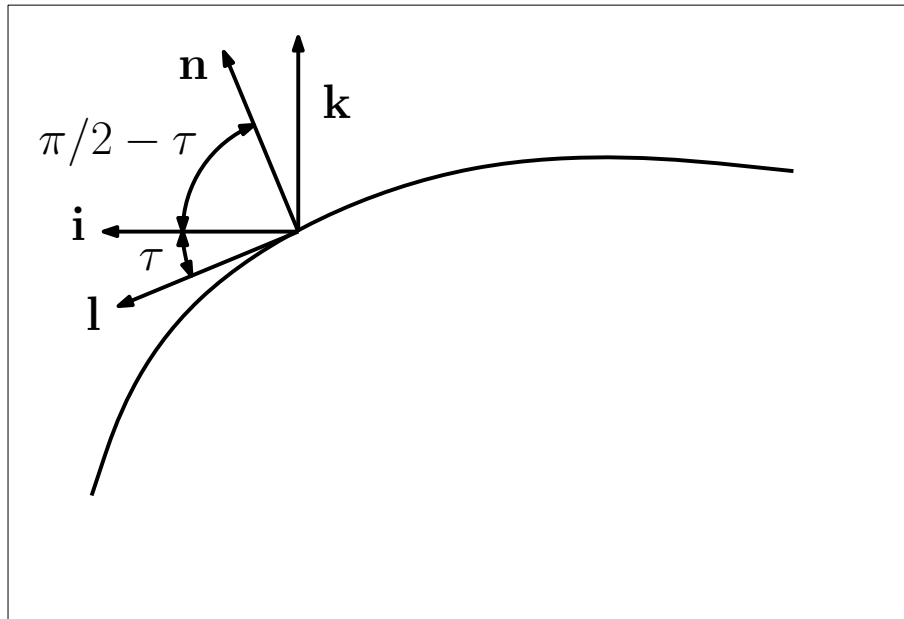
Figure 2.6: tangential and normal vectors to the membrane for deformed configuration

for fluid and noting the fact that there is no body force, we have

$$\text{div}\mathbf{T}_f = \mathbf{0}. \tag{2.152}$$

In order to use (2.152), we use the definition of trace for a 3rd order tensor. Suppose $\mathbf{a},\mathbf{b}$ and $\mathbf{c}$ are 3 arbitrary vectors. By using the definition of trace for a 3rd order tensor we get

$$\text{tr}(\mathbf{a} \otimes \mathbf{b} \otimes \mathbf{c}) = (\mathbf{b} \cdot \mathbf{c})\mathbf{a} = (\mathbf{a} \otimes \mathbf{b})\mathbf{c}, \tag{2.153}$$

where we have used the property of tensor product. Now, by using equation $(\textbf{??})_2$ and (2.152)

$$\text{tr}(\text{grad}(-p_f\mathbf{I})) = \mathbf{0}. \tag{2.154}$$

By using tensor algebra [26] and (2.153) we have

$$\text{tr}\left(\mathbf{I} \otimes \text{grad}(p_f)\right) = \mathbf{I}(\text{grad}(p_f)) = \text{grad}(p_f) = \mathbf{0}, \tag{2.155}$$

which means that the fluid pressure is constant at equilibrium in the deformed configuration. Moreover, since the fluid is considered to be incompressible, the volume

of the fluid is fixed which puts a constraint on the solutions to be obtained

$$V = V_0, \tag{2.156}$$

where V and V_0 are the current and referential volume of the fluid, respectively.

2.4 Governing Ordinary Differential Equations

For obtaining the governing ordinary differential equations, we use the assumption that the contact with the indenter and flat support is frictionless. Therefore, the traction resulted from contact with rigid indenter and support is normal to the membrane

$$\mathbf{f}_c = -p_c\mathbf{n}, \tag{2.157}$$

where $\mathbf{f}_c$ is the contact traction, p_c is the contact pressure and $\mathbf{n}$ is the unit normal to the membrane. The minus sign is due to the assumed direction for the normal to the membrane which is shown in Figure 2.6. We also use the fact that the contact pressure is zero in the part of the membrane that is not in contact with indenter or support.

By substituting (2.149), (2.151) and (2.157) into (2.126) we obtain the following equation

$$\frac{1}{R\sin\phi}(w_\lambda\cos\phi\mathbf{l} - w_\mu\mathbf{i}) + \frac{1}{R}(w_\lambda'\mathbf{l} + w_\lambda\mathbf{l}') + \lambda\mu(p_f - p_c)\mathbf{n} = \mathbf{0}. \tag{2.158}$$

For projecting (2.158) in the $\mathbf{l}$ and $\mathbf{n}$ directions, we need to calculate the vector products such as $\mathbf{l} \cdot \mathbf{i}$, $\mathbf{n} \cdot \mathbf{i}$, etc. Since $\mathbf{l}$ and $\mathbf{n}$ are orthonormal vectors

$$\mathbf{l} \cdot \mathbf{l} = \mathbf{n} \cdot \mathbf{n} = 1, \tag{2.159}$$

$$\mathbf{l} \cdot \mathbf{n} = 0. \tag{2.160}$$

Furthermore, from Figure (2.6) we have

$$\mathbf{l} = \cos\tau\mathbf{i} - \sin\tau\mathbf{k}, \tag{2.161}$$

$$\mathbf{n} = \sin\tau\mathbf{i} + \cos\tau\mathbf{k}. \tag{2.162}$$

By taking the derivative of (2.161) with respect to ϕ

$$\mathbf{l}' = \frac{\partial \mathbf{l}}{\partial \phi} = -\tau' \sin \tau \mathbf{i} - \tau' \cos \tau \mathbf{k}. \tag{2.163}$$

Therefore, from (2.163), (2.161) and (2.162) we have

$$\mathbf{l}' \cdot \mathbf{n} = -\tau', \tag{2.164}$$

$$\mathbf{l}' \cdot \mathbf{l} = 0, \tag{2.165}$$

$$\mathbf{l} \cdot \mathbf{i} = \cos \tau, \tag{2.166}$$

$$\mathbf{n} \cdot \mathbf{i} = \sin \tau. \tag{2.167}$$

Using these relations, by projecting (2.158) in the orthogonal directions $\mathbf{l}$ and $\mathbf{n}$ we get

$$\frac{1}{\sin \phi}(w_\lambda \cos \phi - w_\mu \cos \tau) + w_\lambda' = 0, \tag{2.168}$$

$$-\frac{w_\mu \sin \tau}{\sin \phi} - w_\lambda \tau' + \lambda \mu R(p_f - p_c) = 0. \tag{2.169}$$

Since strain energy is a function of λ and μ, we know

$$w_\lambda' = w_{\lambda\lambda}\lambda' + w_{\lambda\mu}\mu'. \tag{2.170}$$

Also, for computing the μ', we take the derivative of (2.39) with respect to ϕ

$$\mu' = \frac{1}{R \sin^2 \phi} \left(\sin \phi (r' \sin \psi + r\psi' \cos \psi) - r \sin \psi \cos \phi \right). \tag{2.171}$$

Using equations (2.49), (2.50) and (2.39), we can simplify the above equation to the following form

$$\mu' = \frac{\lambda \cos \tau - \mu \cos \phi}{\sin \phi}. \tag{2.172}$$

Substituting (2.172) into (2.170), we can simplify (2.168) and (2.169) into two ordinary differential equations for λ and τ

$$\lambda' = \frac{(w_\mu - \lambda w_{\lambda\mu}) \cos \tau - (w_\lambda - \mu w_{\lambda\mu}) \cos \phi}{w_{\lambda\lambda} \sin \phi}, \tag{2.173}$$

$$\tau' = \frac{\lambda \mu R(p_f - p_c)}{w_\lambda} - \frac{w_\mu \sin \tau}{w_\lambda \sin \phi}. \tag{2.174}$$

From Figure 2.1

$$u = r \sin \psi, \tag{2.175}$$

$$h = r \cos \psi + h_d, \tag{2.176}$$

where h_d is the indenter height measured from the ground. By taking the derivative of these equations with respect to ϕ we obtain

$$u' = r' \sin \psi + r\psi' \cos \psi, \tag{2.177}$$

$$h' = r' \cos \psi - r\psi' \sin \psi. \tag{2.178}$$

By substituting (2.49) and (2.50) into (2.177) and (2.178) and after simplification we have the following ordinary differential equations for u and h

$$u' = \lambda R \cos \tau, \tag{2.179}$$

$$h' = -\lambda R \sin \tau. \tag{2.180}$$

Equations (2.173), (2.174), (2.179) and (2.180) are 4 coupled ordinary differential equations. The boundary conditions that are coming from the geometry of the membrane and shape of the indenter are

$$\tau(\phi = 0) = 0, \tag{2.181}$$

$$u(\phi = 0) = 0, \tag{2.182}$$

$$h(\phi = 0) = h_d, \tag{2.183}$$

$$u(\phi = \pi) = 0, \tag{2.184}$$

$$h(\phi = \pi) = 0, \tag{2.185}$$

$$\tau(\phi = \pi) = \pi. \tag{2.186}$$

Also, due to the incompressibility condition for fluid, the volume enclosed by the membrane must be preserved.

It should be noted that μ is updated by values of u and ϕ with the following equation which is based on (2.39)

$$\mu = \frac{u}{R \sin \phi}. \tag{2.187}$$

We can use the above equation to simplify (2.173) in the following way. First we take the derivative of (2.187) with respect to ϕ and by using (2.179) after simplification we get

$$\mu \cos \phi = \lambda \cos \tau - \mu' \sin \phi. \tag{2.188}$$

By substituting the above equation into (2.173) and simplifying, we obtain

$$(w_{\lambda\lambda}\lambda' + w_{\lambda\mu}\mu') \sin \phi + w_\lambda \cos \phi = w_\mu \cos \tau, \tag{2.189}$$

and finally the above equation simplifies to

$$(w_\lambda \sin \phi)' = w_\mu \cos \tau. \tag{2.190}$$

The above equation can be analytically solved in the region where the membrane is in contact with the cylindrical part of the indenter. This result is used in the section Section 2.6.

2.5   Evaluation of Equilibrium After Penetration

In this section, we consider the equilibrium solutions after penetration. After the penetration occurs, assume the membrane is partially in contact with the cylindrical part of the indenter in the domain $\phi \in [0, \bar{\phi}]$ where $\bar{\phi}$ is the transition angle between the contacting and non-contacting part. At $\phi = \bar{\phi}$, we know $\tau = -\frac{\pi}{2}$; therefore, smoothness of the solution due to pressure implies that there is a domain $[\bar{\phi}, \bar{\phi} + \epsilon]$ for some $\epsilon > 0$ such that $\tau < 0$ in that domain

$$\tau < 0, \quad \bar{\phi} \leq \phi \leq \bar{\phi} + \epsilon. \tag{2.191}$$

Moreover, it can be shown that by multiplying (2.174) by $w_\lambda \sin \phi \cos \tau$ and using (2.190) we obtain

$$(w_\lambda \sin \phi \sin \tau)' = \lambda \mu R(p_f - p_c) \sin \phi \cos \tau, \tag{2.192}$$

and by using (2.179) and (2.39) we get

$$R(w_\lambda \sin \phi \sin \tau)' = uu'(p_f - p_c). \tag{2.193}$$

The above equation can be integrated in the non-contacting region of the punctured membrane where $p_c = 0$

$$Rw_\lambda \sin\phi \sin\tau = \frac{1}{2}p_f u^2 + \alpha, \qquad (2.194)$$

where α is a constant. Noting the fact that at the punctured membrane $w_\lambda = 0$ at $u = \rho$ we obtain

$$Rw_\lambda \sin\phi \sin\tau = \frac{1}{2}p_f(u^2 - \rho^2). \qquad (2.195)$$

This final equation basically show the equilibrium of a portion of the membrane which is cut by a circumferential circular curve. Using this equation for the domain $[\bar{\phi}, \bar{\phi}+\epsilon]$ which is in the non-contacting region of the punctured membrane and noticing $u > \rho$ in this region, we conclude

$$\tau > 0, \quad \bar{\phi} \le \phi \le \bar{\phi} + \epsilon. \qquad (2.196)$$

Equations (2.191) and (2.196) contradict each other and this shows that at the punctured state, the tangent plane of the membrane can not be continuous at $\bar{\phi}$; however, the fluid pressure must have made the membrane smooth. Based on this observation, we conclude that the fluid pressure must drop to zero after penetration occurs and the fluid escapes. This conclusion and the equilibrium equations (2.190) and (2.195) imply that

$$w_\lambda = w_\mu = 0, \quad \bar{\phi} \le \phi \le \pi. \qquad (2.197)$$

Based on the above discussion, we conclude that after puncturing occurs, the membrane will assume a configuration in which the energy is only stored in the domain $\phi \in [0, \bar{\phi}]$ and the non-contacting portion will be slack with $\lambda = \mu = 1$. Figure (2.7) shows this configuration and the transition angle $\bar{\phi}$ can be computed as

$$\bar{\phi} = \arcsin(\bar{\rho}), \qquad (2.198)$$

where

$$\bar{\rho} = \frac{\rho}{R}, \qquad (2.199)$$

is the non-dimensional indenter radius.
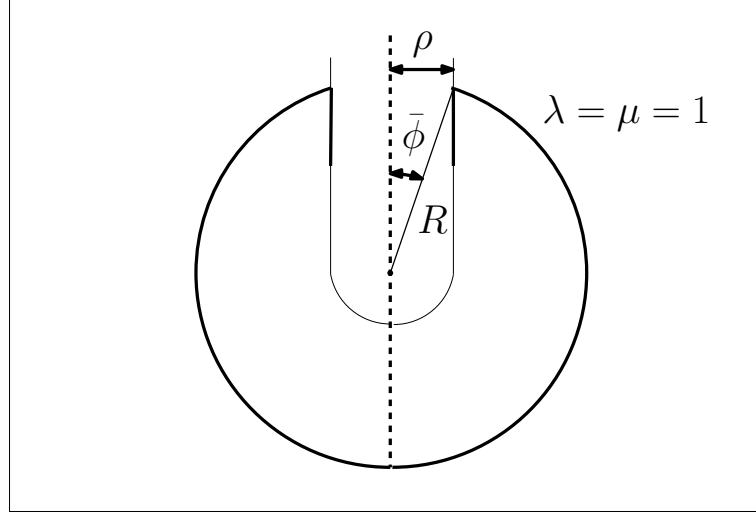
Figure 2.7: The configuration that the membrane assumes after penetration occurs

2.6 Evaluation of Energy of the Penetrated State

In this part we evaluate the energy stored in the punctured membrane. At this state, the fluid pressure is zero and energy vanish everywhere except the part of the membrane which is in contact with the indenter. Since the energy of the membrane is per referential area, we have

$$E_p = \int_\Gamma w(\lambda,\mu)\mathrm{d}A = \int_{\theta=0}^{2\pi}\int_{\phi=0}^{\bar\phi} w(\lambda,\mu)R^2 \sin\phi\mathrm{d}\theta\mathrm{d}\phi = 2\pi R^2 \int_{\phi=0}^{\bar\phi} w(\lambda,\mu)\sin\phi\mathrm{d}\phi, \tag{2.200}$$

where E_p is the stored energy in the membrane at the penetrated state and $\bar\phi$ is given in (2.198). In the contacting part with the indenter $\tau = -\frac{\pi}{2}$; therefore, by substitution into (2.190) we obtain

$$w_\lambda \sin\phi = c, \quad \phi \in [0,\bar\phi], \tag{2.201}$$

where c is a constant. Furthermore, we know that $w_\lambda = 0$ at $\phi = 0$ since this point is a free end; therefore, we must have $c = 0$ which means

$$w_\lambda = 0, \ \phi \in [0,\bar\phi]. \tag{2.202}$$

The above result makes it possible to compute λ as a function of μ and therefore we can express the strain energy as a function of μ in this region. By substituting

(2.202) into (2.81)

$$F'(J) = -\frac{1}{\mu}, \tag{2.203}$$

and we can substitute the above equation into (2.82) to get

$$w_\mu = 2G\left(1 - \frac{\lambda}{\mu}\right) = 2G\left(1 - \frac{v(\mu)}{\mu}\right), \tag{2.204}$$

where $v(\mu)$ is the natural width under uniaxial stress introduced in (2.102). Furthermore, the areal dilation can be expressed in the following form

$$J = \hat{J}(\mu) = \lambda\mu = v(\mu)\mu. \tag{2.205}$$

By substituting (2.205) into (2.204) we get

$$f(\mu) = \frac{\partial \hat{w}(\mu)}{\partial \mu} = 2G\left(1 - \frac{\hat{J}(\mu)}{\mu^2}\right), \tag{2.206}$$

where $f(\mu)$ is the uniaxial stress in the μ direction. Substituting (2.111) into (2.206) and by partial fraction decomposition we get

$$\frac{\partial \hat{w}(x)}{\partial x} = 2G\left(1 - \frac{J_0}{J_0 - 1}\left(\frac{1}{x} - \frac{1}{J_0 - 1 + x}\right)\right). \tag{2.207}$$

After integrating the above equation for the domain $0 < \phi \le \bar{\phi}$ where x is changing from $\mu = 1$ to an intermediate value μ, we get

$$\hat{w}(\mu) - \hat{w}(1) = 2G\left(x - \frac{J_0}{J_0 - 1}\left(\ln x - \ln\left(J_0 - 1 + x\right)\right)\right)\Big|_1^\mu. \tag{2.208}$$

By imposing the condition $\hat{w}(1) = 0$ which means the energy is zero in the absence of stretch, we finally find the strain energy function as a function of μ for the domain $0 < \phi \le \bar{\phi}$ at the penetrated state in the following form

$$\hat{w}(\mu) = 2G\left(\mu - 1 - \frac{J_0}{J_0 - 1}\left(\ln \mu - \ln\left(J_0 - 1 + \mu\right) + \ln J_0\right)\right), \tag{2.209}$$

By substituting the above equation into (2.200) we have

$$E_p = 2\pi R^2 \int_{\phi=0}^{\bar{\phi}} \hat{w}(\mu) \sin\phi \, \mathrm{d}\phi. \tag{2.210}$$

In this region, from (2.39) we have

$$\mu = \frac{\rho}{R\sin\phi} = \frac{\bar{\rho}}{\sin\phi}, \tag{2.211}$$

where $\bar{\rho} = \frac{\rho}{R}$ is the non-dimensional size of the indenter. By using (2.211) we can change the variable of integration from ϕ to μ. Also, from (2.211) we notice that as $\phi \to 0$, $\mu \to \infty$ and after simplification, the integral of (2.210) can be written as

$$E_p = 2\pi R^2 \bar{\rho}^2 \int_1^\infty \frac{\hat{w}(\mu)\mathrm{d}\mu}{\mu^2\sqrt{\mu^2 - \bar{\rho}^2}}. \tag{2.212}$$

Puncturing is possible only if the punctured energy is finite. The necessary (but not sufficient) condition for the above integral to exist is that the integrand must go to zero as $\mu \to \infty$. From (2.209), it is clear that as $\mu \to \infty$, $\hat{w}(\mu) \to 2G\mu$ which indicates that the integrand will approach to zero and this necessary condition is satisfied. By combining (2.209) and (2.212), the energy can be written in the following form

$$E_p = A\bar{\rho}^2 G \left(Q_1 - \frac{J_0}{J_0 - 1}(Q_2 \ln J_0 + Q_3) \right), \tag{2.213}$$

where $A = 4\pi R^2$ is the referential area and Q_1, Q_2 and Q_3 are

$$Q_1 = \int_1^\infty \frac{\mu - 1}{\mu^2\sqrt{\mu^2 - \bar{\rho}^2}}\mathrm{d}\mu, \tag{2.214}$$

$$Q_2 = \int_1^\infty \frac{1}{\mu^2\sqrt{\mu^2 - \bar{\rho}^2}}\mathrm{d}\mu, \tag{2.215}$$

$$Q_3 = \int_1^\infty \frac{1}{\mu^2\sqrt{\mu^2 - \bar{\rho}^2}} \ln\left(\frac{\mu}{J_0 - 1 + \mu}\right)\mathrm{d}\mu. \tag{2.216}$$

For evaluating Q_1, by using integration by parts we have

$$Q_1 = \left.\frac{\sqrt{\mu^2 - \bar{\rho}^2}}{\bar{\rho}^2\mu}(\mu - 1)\right|_1^{\hat{\mu}\to\infty} - \int_1^{\hat{\mu}\to\infty} \frac{\sqrt{\mu^2 - \bar{\rho}^2}}{\bar{\rho}^2\mu}\mathrm{d}\mu. \tag{2.217}$$

Also, by evaluating the second integral we get

$$Q_1 = \frac{\sqrt{\mu^2 - \bar{\rho}^2}}{\bar{\rho}^2 \mu}(\mu - 1)\Big|_1^{\hat{\mu}\to\infty} - \frac{1}{\bar{\rho}^2}\left(\sqrt{\mu^2 - \bar{\rho}^2} + \bar{\rho}\arctan\left(\frac{\bar{\rho}}{\sqrt{\mu^2 - \bar{\rho}^2}}\right)\right)\Big|_1^{\hat{\mu}\to\infty}. \tag{2.218}$$

By taking the limits, the above integral simplifies to the following form

$$Q_1 = \frac{1}{\bar{\rho}^2}\left(\sqrt{1 - \bar{\rho}^2} + \bar{\rho}\arctan\left(\frac{\bar{\rho}}{\sqrt{1 - \bar{\rho}^2}}\right)\right). \tag{2.219}$$

Moreover, after evaluating Q_2 we obtain

$$Q_2 = \frac{\sqrt{\mu^2 - \bar{\rho}^2}}{\bar{\rho}^2 \mu}\Big|_1^{\hat{\mu}\to\infty}, \tag{2.220}$$

and after taking the limits

$$Q_2 = \frac{1 - \sqrt{1 - \bar{\rho}^2}}{\bar{\rho}^2}. \tag{2.221}$$

For evaluating Q_3, using integration by parts yields

$$Q_3 = \ln\left(\frac{\mu}{J_0 - 1 + \mu}\right)\frac{\sqrt{\mu^2 - \bar{\rho}^2}}{\bar{\rho}^2 \mu}\Big|_1^{\hat{\mu}\to\infty} - \int_1^{\hat{\mu}\to\infty}\frac{\sqrt{\mu^2 - \bar{\rho}^2}}{\bar{\rho}^2 \mu}\frac{J_0 - 1}{\mu(J_0 - 1 + \mu)}d\mu. \tag{2.222}$$

Evaluating the second integral and taking the limits, yields the following result for Q_3

$$Q_3 = \ln(J_0)\frac{t}{\bar{\rho}^2} + \frac{s\ln\left(\frac{(b-s)(b+1)}{\bar{\rho}^2 + b - st}\right) + b(1 - t) - \bar{\rho}\arctan\left(\frac{\bar{\rho}}{t}\right)}{b\bar{\rho}^2}, \tag{2.223}$$

where

$$t = \sqrt{1 - \bar{\rho}^2}, \tag{2.224}$$

$$s = \sqrt{b^2 - \bar{\rho}^2}, \tag{2.225}$$

$$b = J_0 - 1. \tag{2.226}$$

In summary, the punctured energy E_p is computed as

$$\frac{E_p}{AG} = Q_1 - \frac{J_0}{J_0 - 1}\left(\ln(J_0)Q_2 + Q_3\right), \tag{2.227}$$

where

$$Q_1 = t + \bar{\rho}\arctan\left(\frac{\bar{\rho}}{t}\right), \tag{2.228}$$

$$Q_2 = 1 - t, \tag{2.229}$$

$$Q_3 = \ln(J_0)t + \frac{s\ln\left(\frac{(b-s)(b+1)}{\bar{\rho}^2+b-st}\right) + b(1-t) - \bar{\rho}\arctan\left(\frac{\bar{\rho}}{t}\right)}{b}, \tag{2.230}$$

$$A = 4\pi R^2. \tag{2.231}$$

Therefore, puncturing for this strain energy in this work is possible and the penetration energy is evaluated from equations (2.227), (2.228), (2.229) and (2.230). The requirement for the non-negativity of the argument of the square root indicates that

$$\bar{\rho} \le \min(J_0 - 1, 1) \tag{2.232}$$

which puts a restriction on the allowable size of the indenter for which the penetrated energy is finite.

We can evaluate this energy in the limit case where $\bar{\rho} \to 0$. After evaluation of this limit we see that

$$\lim_{\bar{\rho}\to 0} E_p = AG, \tag{2.233}$$

which is independent of J_0 and it corresponds to spontaneous cavitation. The following figure shows how the penetration energy changes for different values of $\bar{\rho}$ and J_0. As it can be seen from Figure 2.8, the penetration energy increases as the size of the indenter increases and this is due to the fact that bigger indenter requires more deformation for the penetrated state which translates into more energy. Furthermore, the penetration energy decreases as J_0 increases which indicates that the material becomes less stiff with the increase in J_0. The horizontal dashed line in this figure shows the value obtained from equation (2.233) and there is a good agreement between the numerical result and this analytical formula for $\bar{\rho} \to 0$.
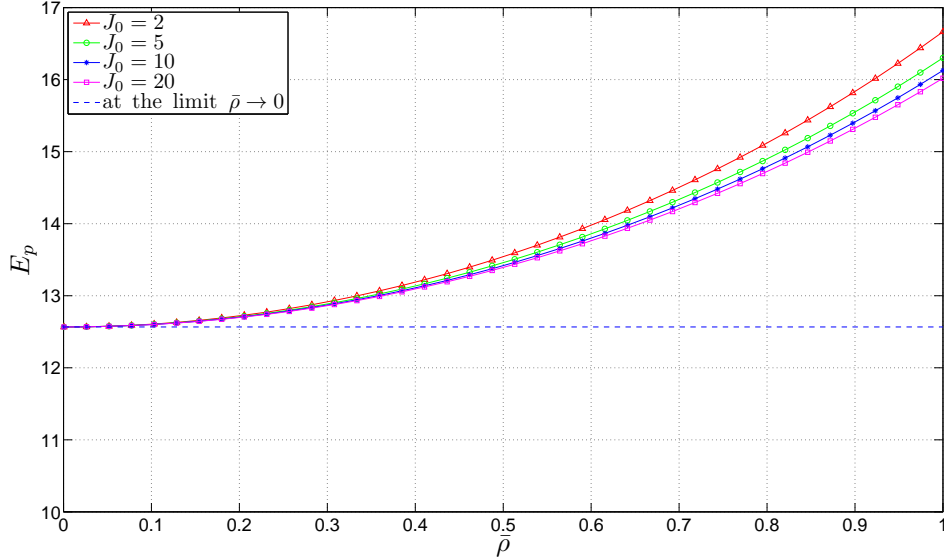
Figure 2.8: penetration energy as a function of $\bar{\rho}$ for different values of J_0. The horizontal dashed line shows the limit of energy when $\bar{\rho} \to 0$

2.7 Failure Criteria

Two failure criteria are considered in this work:

- *Global Failure Due to Energy*: we use the idea that is adopted in fracture mechanics to assume that penetration occurs when the stored energy in the membrane during the indentation exceeds the energy of the punctured membrane since the punctured state has lower energy and is energetically favourable. We only consider the quasistatic process and do not consider the dynamic process associated with the penetration. Also, as stated in the section Section 2.5, the fluid will escape after the penetration occurs and we do not seek any equilibrium solutions after that point.

- *Local Failure Due to Local Loss of Elastic Behaviour*: As stated in the section Section 2.2, when during indentation at some point the dilation becomes bigger than J_0, the material requirement (2.96) is not satisfied and the material is no longer suitable for elasticity. Similarly, in [14] for the same material it is shown that the solution for biaxial loads on a plane sheet is unstable if the square root of the determinant of right Cauchy-Green deformation tensor (J) exceeds J_0. This observation provides an additional insight into the different character of

this strain energy function when $J > J_0$. Therefore the material stops behaving properly and we claim that material fails due to local loss of elastic behaviour when dilation exceeds J_0 and this will give us an additional local failure criteria beside global failure due to energy.

Chapter 3

Numerical Algorithm

3.1 Approximation of Derivatives

From (2.173) and (2.174), at $\phi = 0$ and $\phi = \pi$ the denominator goes to zero and the derivatives for λ and τ can not be computed from these formulas directly. Instead, we use Taylor expansion to approximate the values for λ and τ. By writing the Taylor expansion of $\lambda \sin \phi$ and $\tau \sin \phi$ and by neglecting higher order derivatives

$$\lambda \sin \phi|_{0+\Delta\phi} = \lambda \sin \phi|_0 + \frac{1}{1!} (\lambda' \sin \phi + \lambda \cos \phi)|_0 \Delta\phi + O(\Delta\phi^2), \qquad (3.1)$$

$$\tau \sin \phi|_{0+\Delta\phi} = \tau \sin \phi|_0 + \frac{1}{1!} (\tau' \sin \phi + \tau \cos \phi)|_0 \Delta\phi + O(\Delta\phi^2), \qquad (3.2)$$

and from (2.173) and (2.174) since at $\phi = 0$ we have $\lambda = \mu$, $\tau = 0$ and $p_f = p_c$ (since the membrane is flat at $\phi = 0$), after simplification we obtain

$$\lambda' \sin \phi|_0 = 0, \qquad (3.3)$$

$$\tau' \sin \phi|_0 = 0. \qquad (3.4)$$

By substituting the above results into (3.1) and (3.2), we have

$$\lambda|_{\Delta\phi} \sin \Delta\phi = \lambda|_0 \Delta\phi + O(\Delta\phi^2), \qquad (3.5)$$

$$\tau|_{\Delta\phi} \sin \Delta\phi = \tau|_0 \Delta\phi + O(\Delta\phi^2). \qquad (3.6)$$

Since for small angles we have $\sin \Delta\phi \approx \Delta\phi$, therefore

$$\lambda|_{\Delta\phi} \approx \lambda|_0, \tag{3.7}$$

$$\tau|_{\Delta\phi} \approx \tau|_0, \tag{3.8}$$

which is the approximation that we use for λ and τ at $\Delta\phi$. The same approach is used at $\phi = \pi$ to address the similar issue which leads to the result

$$\lambda|_{\pi-\Delta\phi} \approx \lambda|_\pi, \tag{3.9}$$

$$\tau|_{\pi-\Delta\phi} \approx \tau|_\pi. \tag{3.10}$$

3.2 Initial Inflation

Because we are interested in the deformation of an inflated membrane, we inflate the membrane from initial radius R to radius $r_0 > R$. In this inflation, there is no change in ϕ or θ for the position of material points as shown in Figure 3.1; therefore, we must have

$$\tau = \psi = \phi, \tag{3.11}$$

where ψ and τ are depicted in Figure 2.1. Since $\tau = \phi$ it means $\tau' = 1$. Furthermore,
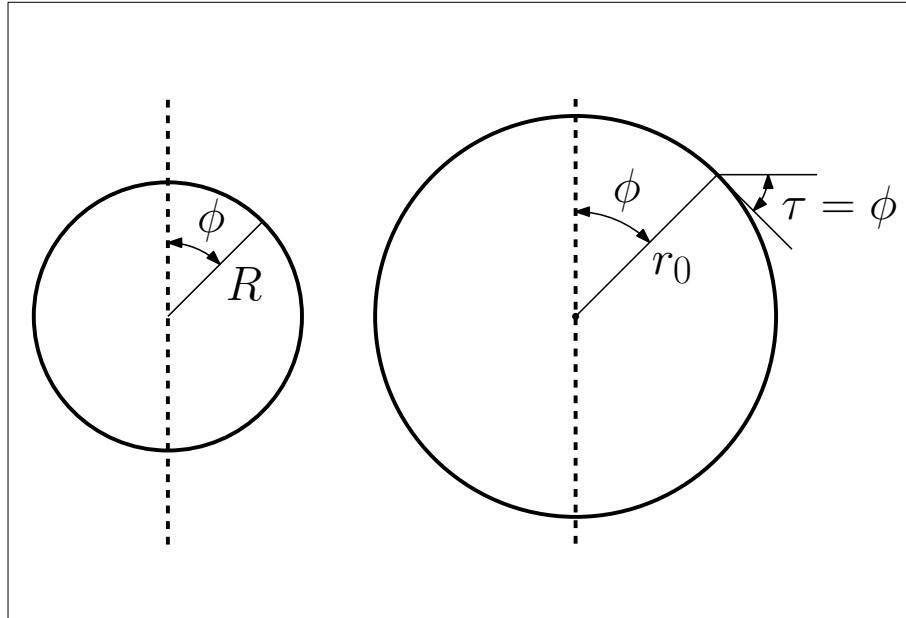
Figure 3.1: reference and inflated configurations

at the initial inflation, $\lambda = \mu = \frac{r_0}{R}$ and also $w_\lambda = w_\mu$. By substituting into (2.174) and noticing that $p_c = 0$ (since there is no contact force at this inflation stage), we can compute the fluid pressure at this inflated configuration in the following form

$$p_{f_0} = \frac{4GR}{r_0^2} \left(1 + \frac{1}{J_0 - 1} \left(\frac{r_0}{R} - \frac{J_0 R}{r_0} \right) \right).$$ (3.12)

3.3   Enclosed Volume

For computing the volume of the enclosed fluid, the following equation is evaluated using the trapezoidal rule

$$V = \int_0^{h_{max}} \pi u^2 \mathrm{d}h - \int_{h_d}^{h_{max}} \pi u^2 \mathrm{d}h,$$ (3.13)

where h_{max} is the maximum height of the membrane and h_d is the height of the indenter, as shown in Figure 3.2.
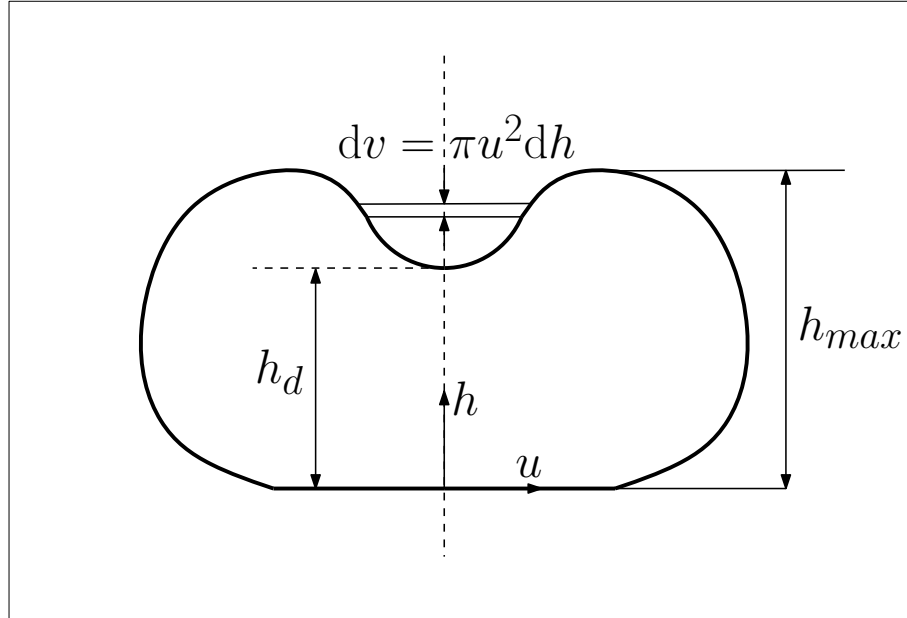
Figure 3.2: disk elements for computation of the volume

3.4 Numerical Method

In order to solve the system of equations for this problem, the multiple shooting method is used which allows us to use the numerical methods of initial value problems. For using multiple shooting method, we divide the domain of the problem $\phi \in [0, \pi]$ into two regions: the upper region which is for $\phi^u \in [0, \frac{\pi}{2}]$ and the lower region which corresponds to $\phi^l \in [\frac{\pi}{2}, \pi]$ and we solve the problem in these two regions and then we match the solution at $\phi = \frac{\pi}{2}$ since the solution must be continuous at this point. For particular results that are presented in the Chapter 4, we divided each domain into 5,000 divisions. We need to control and prescribe a variable to obtain different equilibrium solutions. We have chosen to prescribe the height of the indenter (h_d as shown in Figure 3.2 and we know $0 \leq h_d \leq 2r_0$) since this parameter is easier to prescribe due to the fact that it is monotonically decreasing as the indentation continues. In order to do the integration in these two regions, we need to guess the following set of values

$$\{\phi_{c_1}, \phi_{c_2}, \lambda_0, \lambda_\pi, p_f\} \tag{3.14}$$

where ϕ_{c_1} denotes the transition angle between the contacting part with the indenter and the non-contacting part of the membrane, ϕ_{c_2} denotes the transition angle between the contacting part with the flat support and the non-contacting part of the membrane, λ_0 is the value of λ at $\phi = 0$, λ_π is the value of λ at $\phi = \pi$ and p_f is the fluid pressure.

The ordinary differential equations of this problem and the associated boundary conditions have the following form

$$\frac{\partial y}{\partial \phi} = f(\phi, y), \tag{3.15}$$

$$y(\phi_0) = y_0, \tag{3.16}$$

where y is any of the variables $\{\lambda, u, \tau, h\}$. In order to solve the initial value problems of the above form we use the 4th order Runge-Kutta method with the following

formula

$$y_{n+1} = y_n + \frac{h}{6}\left(K_1 + 2K_2 + 2K_3 + K_4\right), \tag{3.17}$$

$$K_1 = f\left(\phi_n, y_n\right), \tag{3.18}$$

$$K_2 = f\left(\phi_n + \frac{h}{2}, y_n + \frac{h}{2}K_1\right), \tag{3.19}$$

$$K_3 = f\left(\phi_n + \frac{h}{2}, y_n + \frac{h}{2}K_2\right), \tag{3.20}$$

$$K_4 = f\left(\phi_n + h, y_n + hK_3\right), \tag{3.21}$$

where $h = \Delta\phi$ is the step size, y_n and y_{n+1} are the values of y at ϕ_n and ϕ_{n+1}, respectively. After integrating both regions we match the results at $\phi = \frac{\pi}{2}$. Since the values we guess are not the solution, we will have residuals in the following form

$$R_1 = \lambda^u\left(\frac{\pi}{2}; \lambda_0; \phi_{c_1}; p_f\right) - \lambda^l\left(\frac{\pi}{2}; \lambda_\pi; \phi_{c_2}; p_f\right), \tag{3.22}$$

$$R_2 = u^u\left(\frac{\pi}{2}; \lambda_0; \phi_{c_1}; p_f\right) - u^l\left(\frac{\pi}{2}; \lambda_\pi; \phi_{c_2}; p_f\right), \tag{3.23}$$

$$R_3 = \tau^u\left(\frac{\pi}{2}; \lambda_0; \phi_{c_1}; p_f\right) - \tau^l\left(\frac{\pi}{2}; \lambda_\pi; \phi_{c_2}; p_f\right), \tag{3.24}$$

$$R_4 = h^u\left(\frac{\pi}{2}; \lambda_0; \phi_{c_1}; p_f\right) - h^l\left(\frac{\pi}{2}; \lambda_\pi; \phi_{c_2}; p_f\right), \tag{3.25}$$

$$R_5 = V\left(\lambda_0; \lambda_\pi; \phi_{c_1}; \phi_{c_2}; p_f\right) - V_0, \tag{3.26}$$

where $()^u$ and $()^l$ denotes the computed solution in the upper region and lower region, respectively.

The iterative Newton-Raphson method is used to compute the change in guess values in each step in the following form

$$\begin{pmatrix} \frac{\partial R_1}{\partial \lambda_0} & \frac{\partial R_1}{\partial \lambda_\pi} & \frac{\partial R_1}{\partial \phi_{c1}} & \frac{\partial R_1}{\partial \phi_{c2}} & \frac{\partial R_1}{\partial p_f} \\ \frac{\partial R_2}{\partial \lambda_0} & \frac{\partial R_2}{\partial \lambda_\pi} & \frac{\partial R_2}{\partial \phi_{c1}} & \frac{\partial R_2}{\partial \phi_{c2}} & \frac{\partial R_2}{\partial p_f} \\ \frac{\partial R_3}{\partial \lambda_0} & \frac{\partial R_3}{\partial \lambda_\pi} & \frac{\partial R_3}{\partial \phi_{c1}} & \frac{\partial R_3}{\partial \phi_{c2}} & \frac{\partial R_3}{\partial p_f} \\ \frac{\partial R_4}{\partial \lambda_0} & \frac{\partial R_4}{\partial \lambda_\pi} & \frac{\partial R_4}{\partial \phi_{c1}} & \frac{\partial R_4}{\partial \phi_{c2}} & \frac{\partial R_4}{\partial p_f} \\ \frac{\partial R_5}{\partial \lambda_0} & \frac{\partial R_5}{\partial \lambda_\pi} & \frac{\partial R_5}{\partial \phi_{c1}} & \frac{\partial R_5}{\partial \phi_{c2}} & \frac{\partial R_5}{\partial p_f} \end{pmatrix} \begin{pmatrix} d\lambda_0 \\ d\lambda_\pi \\ d\phi_{c1} \\ d\phi_{c2} \\ dp_f \end{pmatrix} = - \begin{pmatrix} R_1 \\ R_2 \\ R_3 \\ R_4 \\ R_5 \end{pmatrix}, \tag{3.27}$$

where R_i are the current residuals and finite difference is used to approximate the derivatives of the residuals. The required change in the guess values are computed from the above equation and the guess values are updated. This process is repeated until convergence is achieved. It should be noted that the above numerical scheme

will work only if our guess values are close to the solution values. Therefore, we start every indentation with the inflated sphere for which we know the following exact solution

$$\phi_{c1} = 0, \tag{3.28}$$

$$\phi_{c2} = \pi, \tag{3.29}$$

$$\lambda_0 = \lambda_\pi = \frac{r_0}{R}, \tag{3.30}$$

$$p_f = p_{f_0}, \tag{3.31}$$

where p_{f_0} is given in (3.12).

Chapter 4

Results

This chapter presents the results obtained by solving equations (2.173), (2.174), (2.179) and (2.180) subject to boundary conditions (2.181) to (2.186) by the numerical procedure outlined in Chapter 3.

4.0.1 Non-Dimensional Variables

We use the following dimensionless variables to present the results

$$\bar{r}_0 = \frac{r_0}{R}, \tag{4.1}$$

$$\bar{\phi}_{c_1} = \frac{\phi_{c_1}}{\pi}, \tag{4.2}$$

$$\bar{\phi}_{c_2} = \frac{\phi_{c_2}}{\pi}, \tag{4.3}$$

$$\bar{\lambda}_0 = \frac{\lambda_0}{\bar{r}_0}, \tag{4.4}$$

$$\bar{\lambda}_\pi = \frac{\lambda_\pi}{\bar{r}_0}, \tag{4.5}$$

$$\bar{p}_f = \frac{p_f}{p_{f_0}}, \tag{4.6}$$

$$\bar{F} = \frac{F}{Gr_0}. \tag{4.7}$$

4.0.2 Sample Indentation Results

The following sample results are obtained for the following values

$$\bar{r}_0 = 1.5, \tag{4.8}$$

$$J_0 = \{10, 15\}, \tag{4.9}$$

$$\bar{\rho} = \{0.1, 0.2, 0.5\}. \tag{4.10}$$

In order to make this document more readable, in this part we present the most interesting results which are for $J_0 = 15$ and extra results for $J_0 = 10$ are presented in the Chapter A in the appendix. The figures in the Appendix A follow a similar trend to the case explained in here. The indentation is continued until the material fails either due to local loss of elastic behaviour or global failure due to penetration as described in Section 2.7. For the particular numbers that are chosen for this part, failure due to local loss of elastic behaviour always happened first and no global failure due to energy was observed. Moreover, we stopped indentation when we observed wrinkling as well since treatment of wrinkling was not the purpose of this work. The horizontal axis in all of the following indentation graphs is the non-dimensional indenter displacement $0 \leq \frac{d}{2r_0} \leq 1$ where d is the indenter displacement as shown in Figure 4.1.
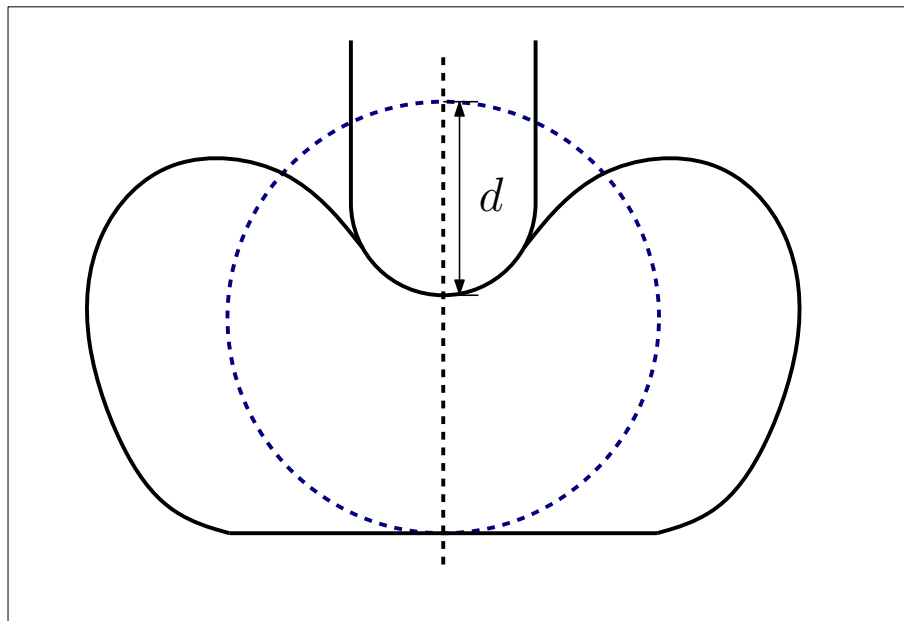
Figure 4.1: indenter displacement

Material in Contact

Figures 4.2 and 4.4, show how $\bar{\phi}_{c_1}$ and $\bar{\phi}_{c_2}$ which are the non-dimensional contacting angles with the indenter and support, respectively are varying during the indentation process. Also, in order to get a better understanding of how much of the material is in contact with the indenter, we can compute the percentage of the referential area in contact with the indenter

$$\frac{A_{\phi_{c_1}}}{A_0} \times 100 = \frac{2\pi R^2 \int_0^{\phi_{c_1}} \sin\phi \, \mathrm{d}\phi}{4\pi R^2} \times 100 = \left(\frac{1 - \cos\phi_{c_1}}{2}\right) \times 100. \qquad (4.11)$$

We can compute the same percentage for the material in contact with the flat support

$$\frac{A_{\phi_{c_2}}}{A_0} \times 100 = \frac{2\pi R^2 \int_{\phi_{c_2}}^{\pi} \sin\phi \, \mathrm{d}\phi}{4\pi R^2} \times 100 = \left(\frac{1 + \cos\phi_{c_2}}{2}\right) \times 100. \qquad (4.12)$$

Figures 4.3 and 4.5 show how these ratios are varying during the indentation. These figures show that the material in contact with the indenter is increasing but this increase is not monotonic and we can see a decline before reaching to failure. This behaviour is not surprising since for example, if we indent a flat piece of material, initially small portion of the material will be in contact with the indenter. As we indent it further, this contacting portion increases; however, we expect that at large indenter displacement only small portion of the material which is extremely stretched will be in contact with the indenter. This shows that the contacting portion of the membrane is not monotonically increasing. Figures 4.4 and 4.5 show a similar trend for the material in contact with the flat support and they show a decline toward the end of the graph which is more noticeable for the case $J_0 = 15$.
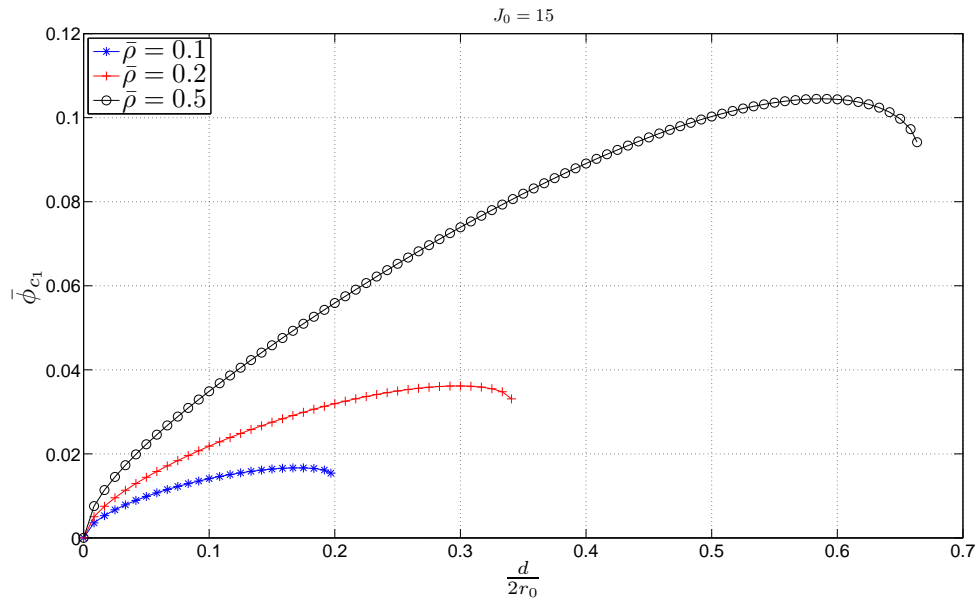
Figure 4.2: $\bar{\phi}_{c_1}$ as a function of non-dimensional displacement for $J_0 = 15$
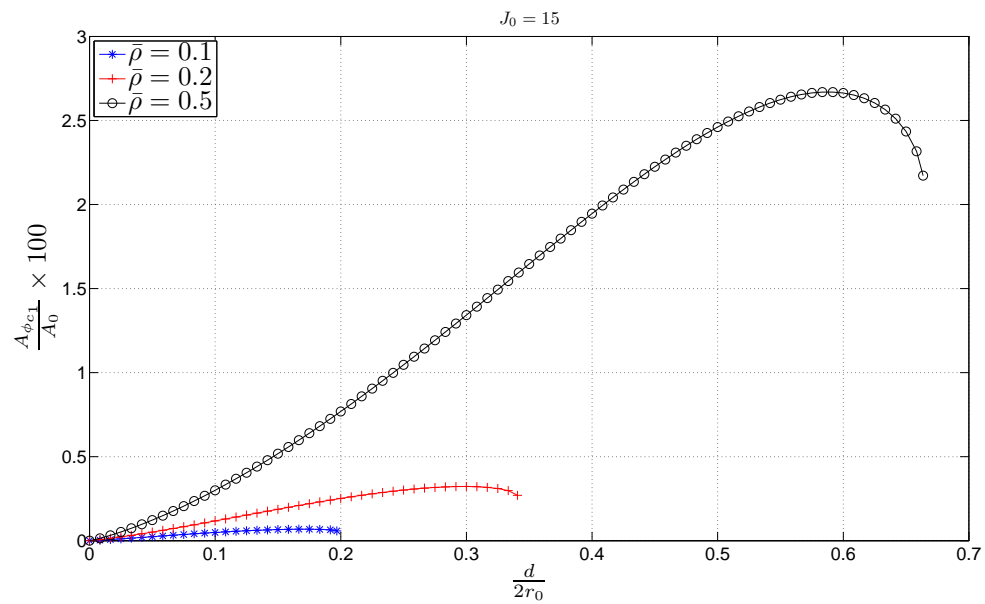
Figure 4.3: $\frac{A_{\phi c_1}}{A_0} \times 100$ as a function of non-dimensional displacement for $J_0 = 15$
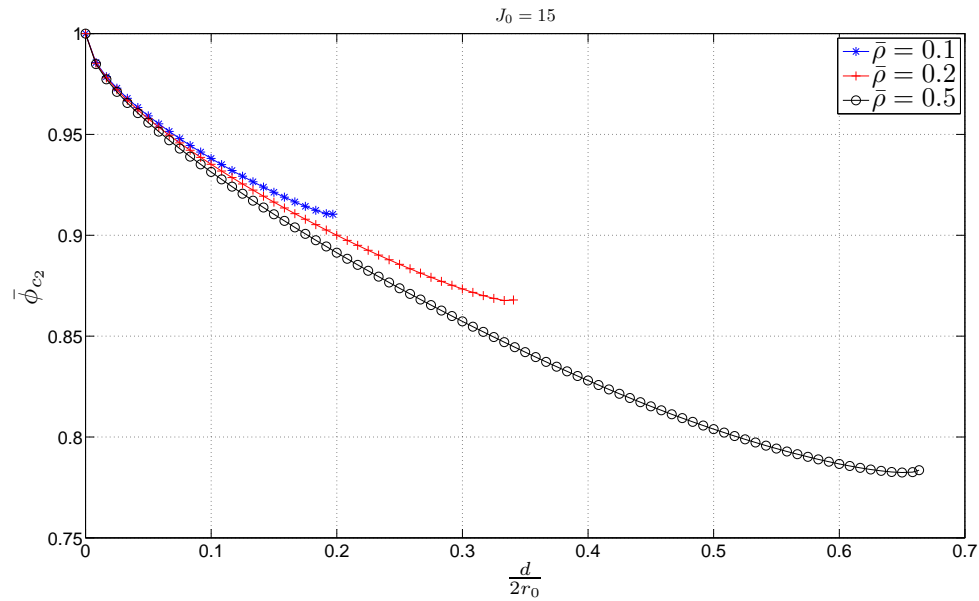
Figure 4.4: $\bar{\phi}_{c_2}$ as a function of non-dimensional displacement for $J_0 = 15$
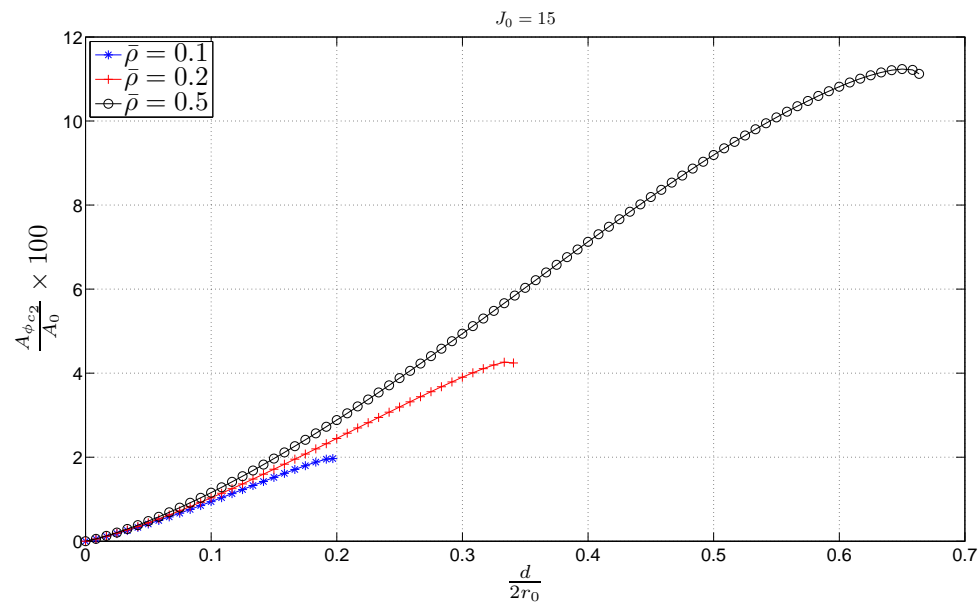
Figure 4.5: $\frac{A_{\phi_{c_2}}}{A_0} \times 100$ as a function of non-dimensional displacement for $J_0 = 15$

Meridional Stretches

We can plot how $\bar{\lambda}_0$ and $\bar{\lambda}_\pi$ (non-dimensional meridional stretches at the poles) are changing during the indentation. Figures 4.6 and 4.7 show these figures. As it can be

seen from figure 4.6, there is an initial decrease in $\bar{\lambda}_0$ which becomes more noticeable as the indenter gets larger. The reason for this decrease is initial flattening of a sphere by the indenter and after the membrane comes more into contact with the indenter and takes the shape of the indenter, the stretch starts to increase. The same reason applies for the decrease of $\bar{\lambda}_\pi$ as shown in Figure 4.7 which continues for larger values of displacement. Furthermore, figure 4.6 shows that as indentation proceeds, the change in $\bar{\lambda}_0$ becomes larger for the same indentation displacement such that close to the point where local loss of elastic behaviour happens $(\max(J) > J_0)$, this graph becomes almost vertical which produces difficulties for finding the numerical solution and the indentation displacement must be reduced constantly to obtain the next solution.
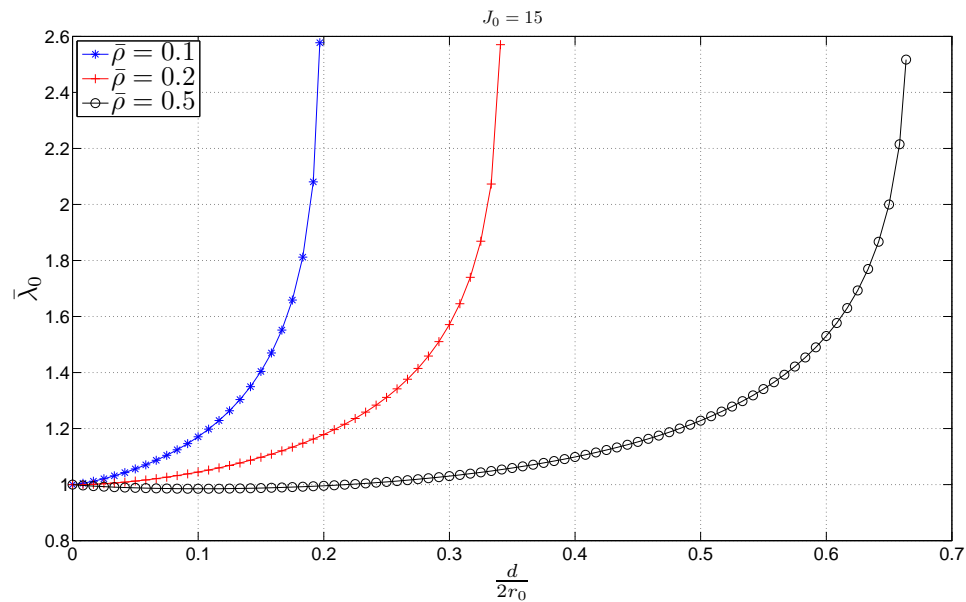
Figure 4.6: $\bar{\lambda}_0$ as a function of non-dimensional displacement for $J_0 = 15$
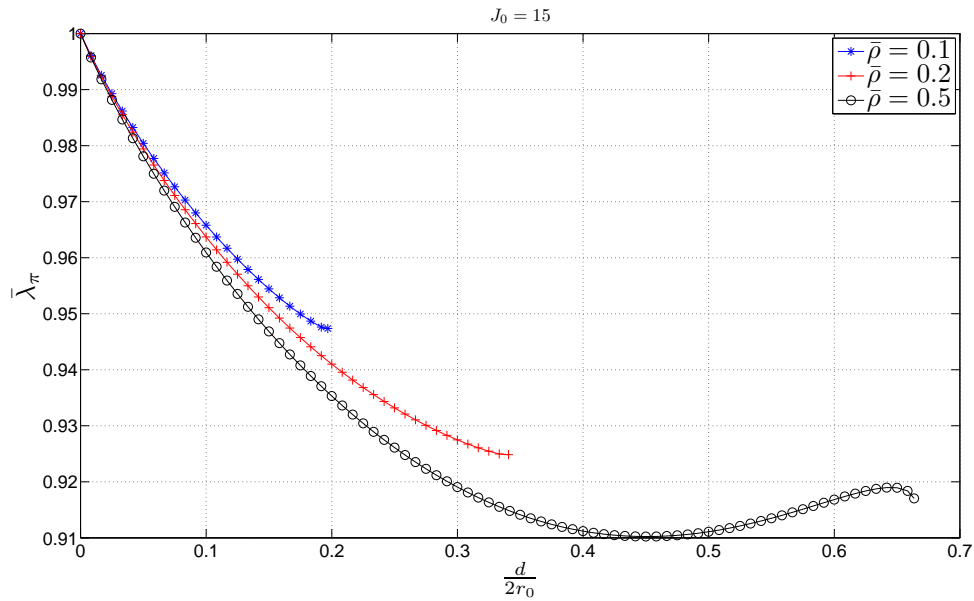
Figure 4.7: $\bar{\lambda}_\pi$ as a function of non-dimensional displacement for $J_0 = 15$

Fluid Pressure

Figure 4.8 shows how the fluid pressure is varying during indentation as a function of indenter displacement. According to this graph, the fluid pressure is increasing as indentation proceeds; however, it starts to decline close to the failure point $(\max(J)$ is close to $J_0)$ which is more noticeable for $\bar{\rho} = 0.5$. This graph shows that for some fluid pressures, there are more than one equilibrium solution and fluid pressure is not a very suitable variable to prescribe for obtaining different equilibrium solutions for the numerical procedure explained in Section 3.4.
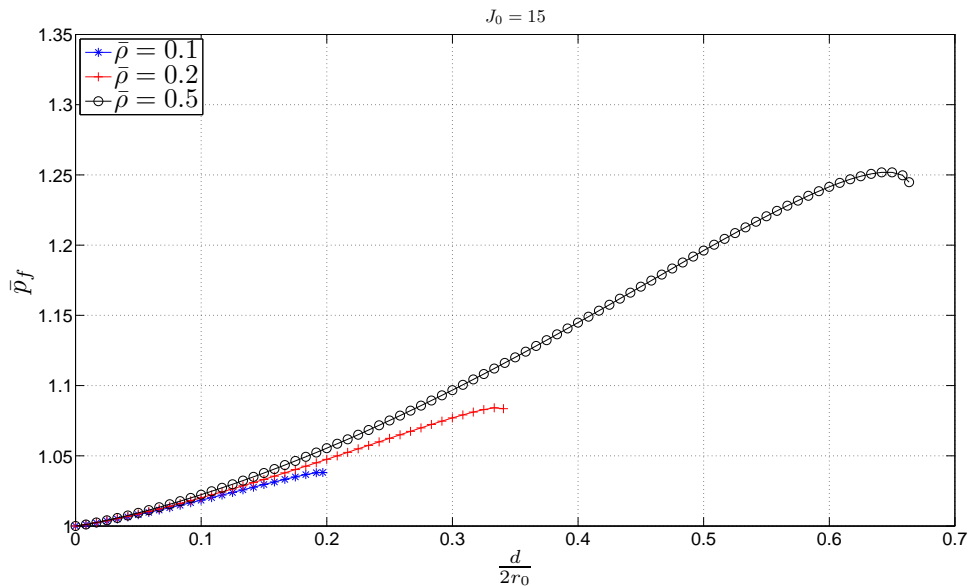
Figure 4.8: $\bar{p}_f$ as a function of non-dimensional displacement for $J_0 = 15$

Indentation Force

Figure 4.9 shows how indentation force is changing during the indentation for $\bar{\rho} = 0.5$ for different values of J_0. The indentation force can be obtained by multiplying fluid pressure (which is equal to the flat support contact pressure) by the deformed area of the contacting region with the support

$$\bar{F} = \frac{1}{Gr_0} p_f \pi u_{\phi_{c_2}}^2, \tag{4.13}$$

where $u_{\phi_{c_2}}$ is the value of u at ϕ_{c_2}. As it can be seen from this graph, as J_0 gets larger the indentation force becomes smaller for the same indenter displacement which indicates that this material becomes less stiff as J_0 gets larger. This is the same conclusion we obtained at the end of Section 2.6 by considering penetrated energy. Furthermore, the indentation force is not monotonically increasing and there can be a decrease close to the failure point which is more visible for $J_0 = 15$. The reason for this decrease is that both fluid pressure and $u_{\phi_{c_2}}$ are dropping close to the failure point as shown in graphs 4.8 and 4.10 (for $J_0 = 15$, $\bar{\rho} = 0.5$).
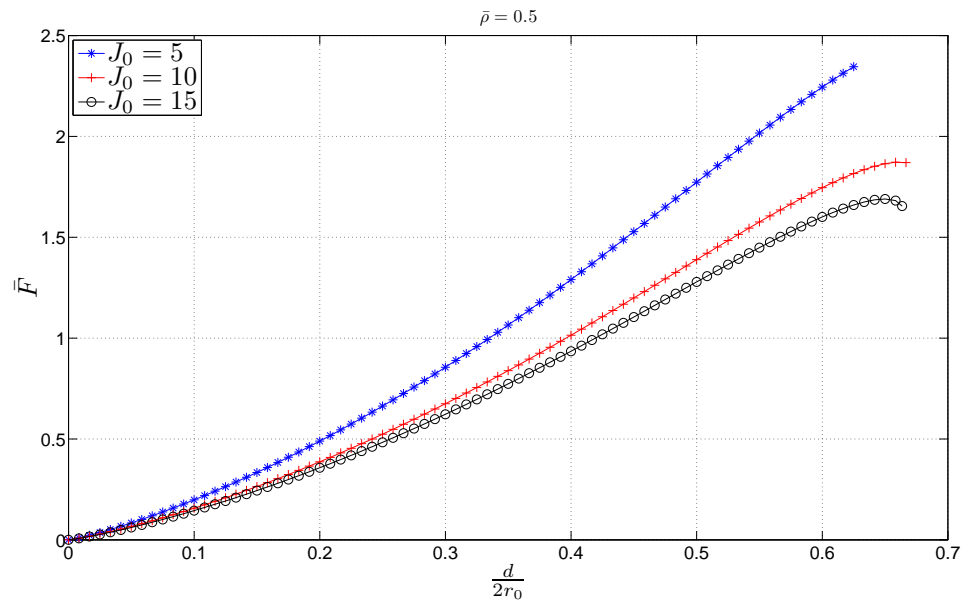
Figure 4.9: $\bar{F}$ as a function of non-dimensional displacement for $\bar{\rho} = 0.5$
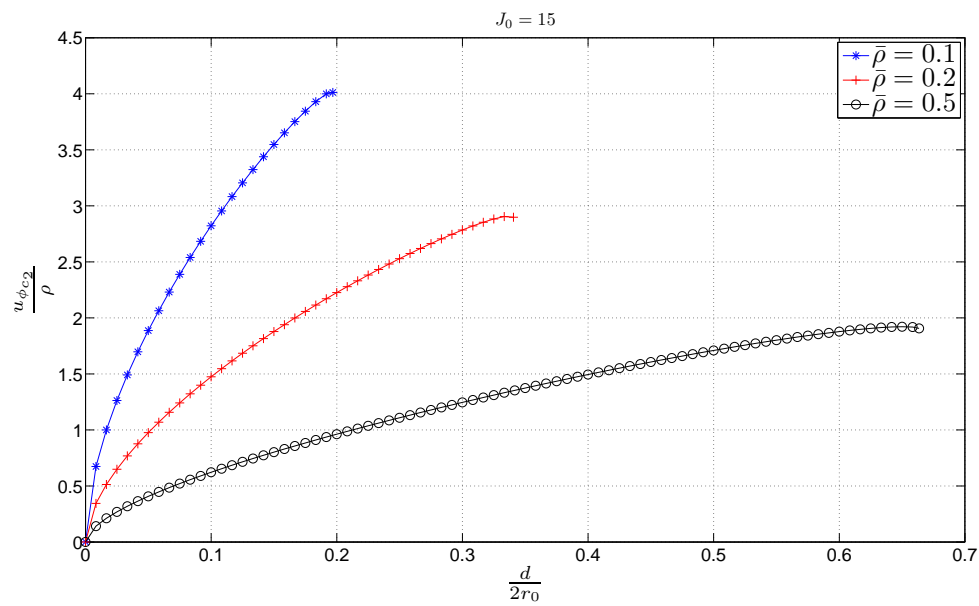
Figure 4.10: $\frac{u_{\phi_{c_2}}}{\rho}$ as a function of non-dimensional displacement for $J_0 = 15$

Energy Ratio

The ratio of the stored energy of the membrane to the energy at the punctured state is shown in Figure 4.11. In [7], it is established that the energy of the membrane is

a strictly increasing function of the indenter displacement (for a flat circular membrane) which is in qualitative agreement with the monotonically increasing behaviour of the result shown in Figure 4.11. Moreover, the energy ratio in this particular example remained less than unity while the failure due to local loss of elastic behaviour happened therefore no global failure due to energy was observed.
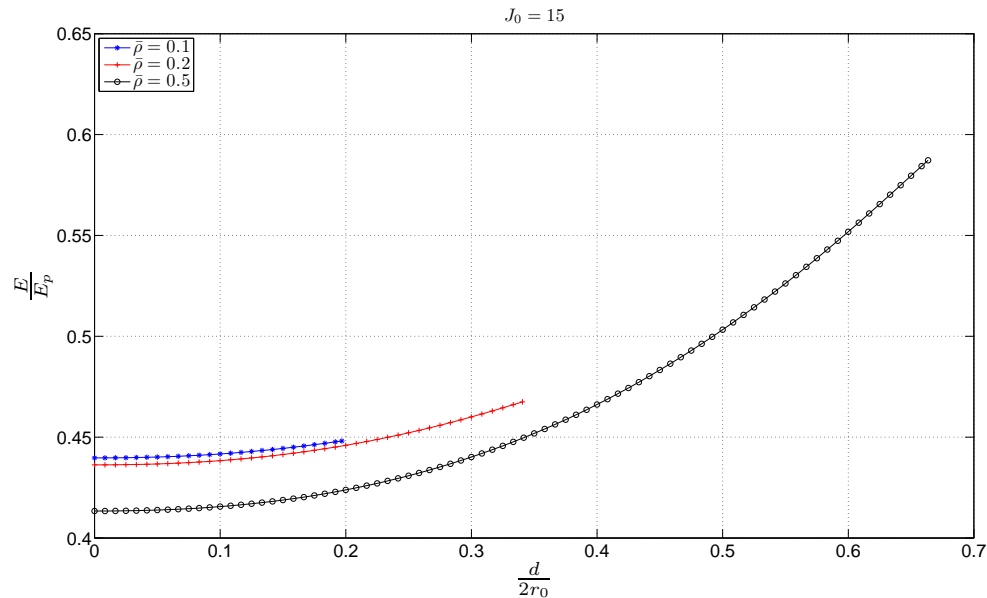
Figure 4.11: Energy ratio $(\frac{E}{E_p})$ as a function of non-dimensional displacement for $J_0 = 15$

Dilation Ratio

Figure 4.12 shows how the ratio of the maximum dilation to J_0 is changing with the indenter displacement. The point that has the maximum dilation always observed to be directly under the tip of the indenter ($\phi = 0$). Close to the point at which local failure occurs, this graph shows the same behaviour as Figure 4.6 for $\bar{\lambda}_0$ and the change in this ratio becomes very large. Due to this behaviour close to the failure point, obtaining the next solution becomes more difficult and as it can be seen it was not possible to get significantly closer to the failure point for the case $J_0 = 15$ and $\bar{\rho} = 0.5$.
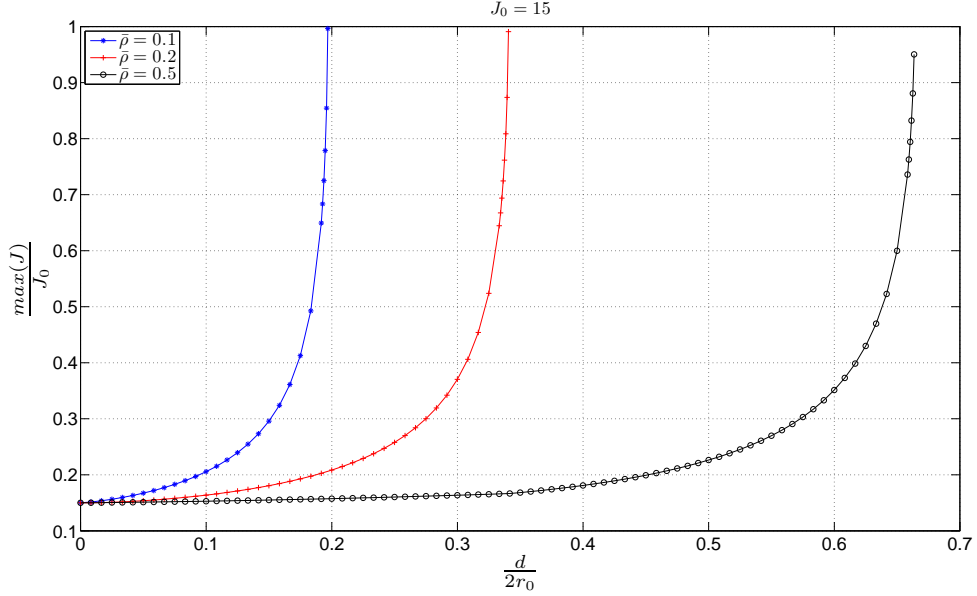
Figure 4.12: Dilation ratio $(\frac{\max(J)}{J_0})$ as a function of non-dimensional displacement for $J_0 = 15$

4.0.3 Constant Pressure Case

We can consider the indentation of a particular membrane that allows the incompressible fluid to pass through the membrane such that the fluid pressure remains constant

$$p_f = p_{f_0}, \tag{4.14}$$

where p_{f_0} is given in (3.12). We present the results in this case for the following sample values

$$\bar{r}_0 = 1.5, \tag{4.15}$$

$$J_0 = \{5, 10\}, \tag{4.16}$$

$$\bar{\rho} = 0.1. \tag{4.17}$$

We stopped the indentation whenever the membrane reached to failure. Also, in some cases we observed wrinkling before the failure and we stopped the indentation; for example, for $J_0 = 5$ and $\bar{\rho} = 0.5$ wrinkling occurred at the indenter displacement of 85% with energy ratio of 9.01% and dilation ratio of 37.97% which is clearly before any mode of failure.

For the constant pressure case, there is no requirement for the membrane to preserve its volume; therefore, volume of the membrane will decrease as shown in Figure 4.13. This figure shows how the ratio of the current volume of the membrane to the initial volume is changing during the indentation.

The energy ratio of the membrane during the indentation is shown in Figure 4.14. This graph shows that when the pressure is kept constant, the energy is reducing and the global mode of failure will not occur during the indentation. Therefore, the only possibility to get global failure is to inflate the membrane to a critical value at which the intact energy of the membrane reaches to the penetrated energy and the membrane fails immediately.

On the other hand, the dilation ratio which is presented in Figure 4.15 shows that this ratio is increasing when the pressure is kept constant. This figure indicates that the membrane is failed locally when this ratio exceeds unity and the point with maximum dilation is again observed to be at $\phi = 0$; i.e., directly under the indenter.
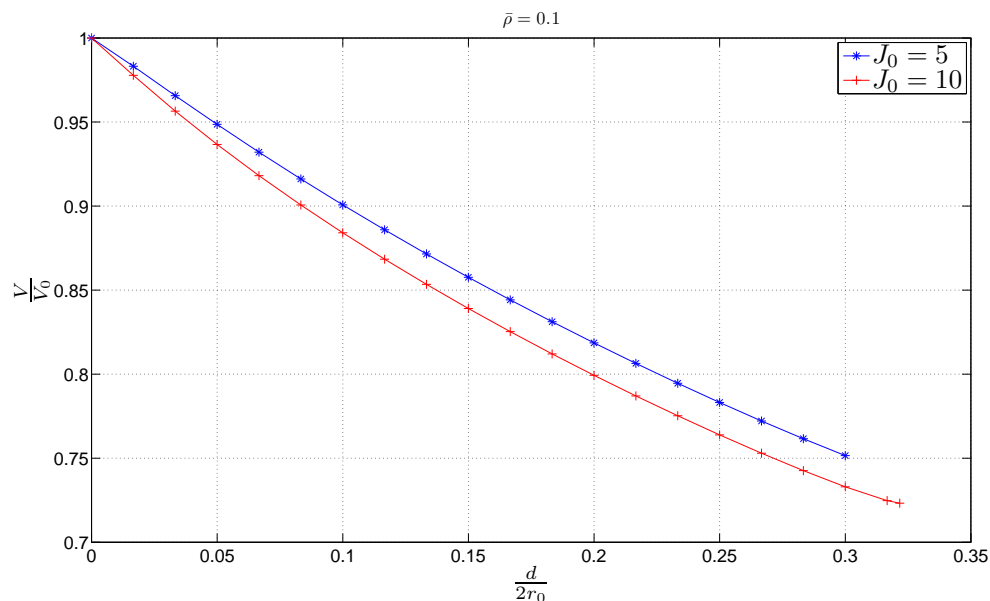
Figure 4.13: Volume ratio $(\frac{V}{V_0})$ as a function of non-dimensional displacement for $\bar{\rho} = 0.1$ for constant pressure case
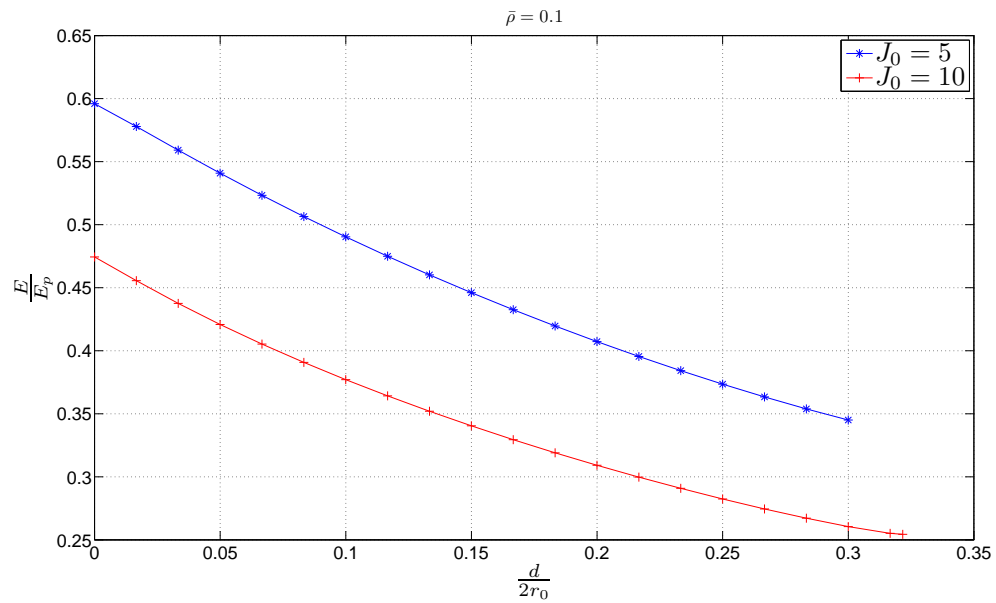
Figure 4.14: Energy ratio $(\frac{E}{E_p})$ as a function of non-dimensional displacement for $\bar{\rho} = 0.1$ for constant pressure case
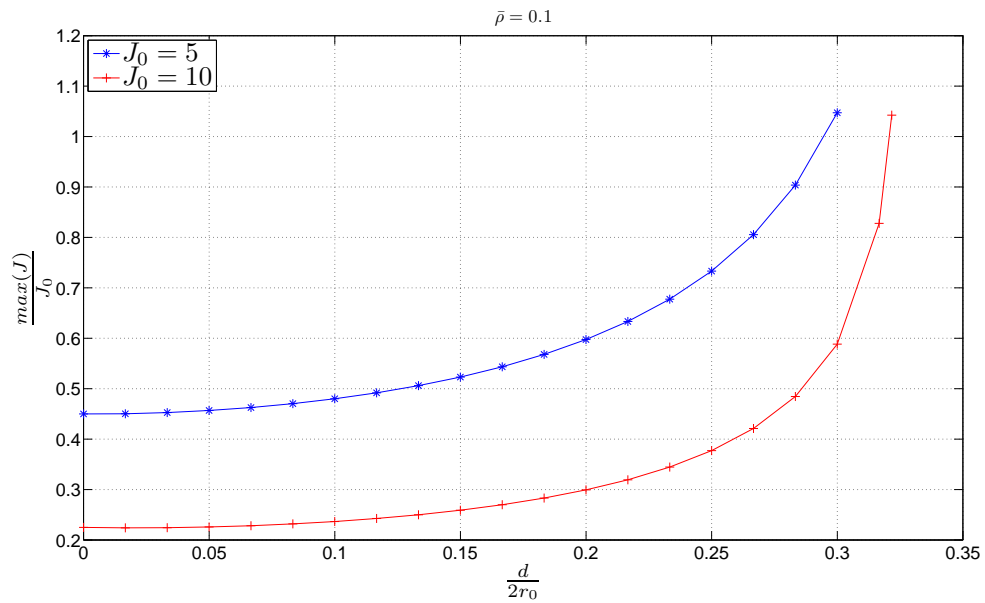
Figure 4.15: Dilation ratio $(\frac{\max(J)}{J_0})$ as a function of non-dimensional displacement for $\bar{\rho} = 0.1$ for constant pressure case

4.0.4   Critical Inflation For Cavitation

We can consider the critical inflation for cavitation ($\bar{\rho} \to 0$) at which failure occurs immediately with zero indenter displacement as a function of J_0. Figure 4.16 shows this figure and indicates the corresponding mode of failure as well. The region under this graph indicates the inflation values for each J_0 that failure does not occur immediately. As it can be seen from this graph for approximately $J_0 \leq 2.05$, the failure occurs due to local loss of elastic behaviour and the corresponding portion of the curve (blue curve) is determined by $\frac{r0}{R} = \sqrt{J_0}$. For greater values of J_0, global failure mode due to energy determines the critical inflation which is obtained numerically. This graph indicates that for small values of J_0, as inflation increases, the value of $\max(J) = (\frac{r_0}{R})^2$ reaches to J_0 before the membrane reaches to the inflation at which the inflated energy equals to the penetration energy. However, for larger values of J_0, at the inflation for which immediate failure due to energy happens, the value of $\max(J) = (\frac{r_0}{R})^2$ is smaller than J_0 therefore the critical inflation is dominated by the global mode of failure due to energy.
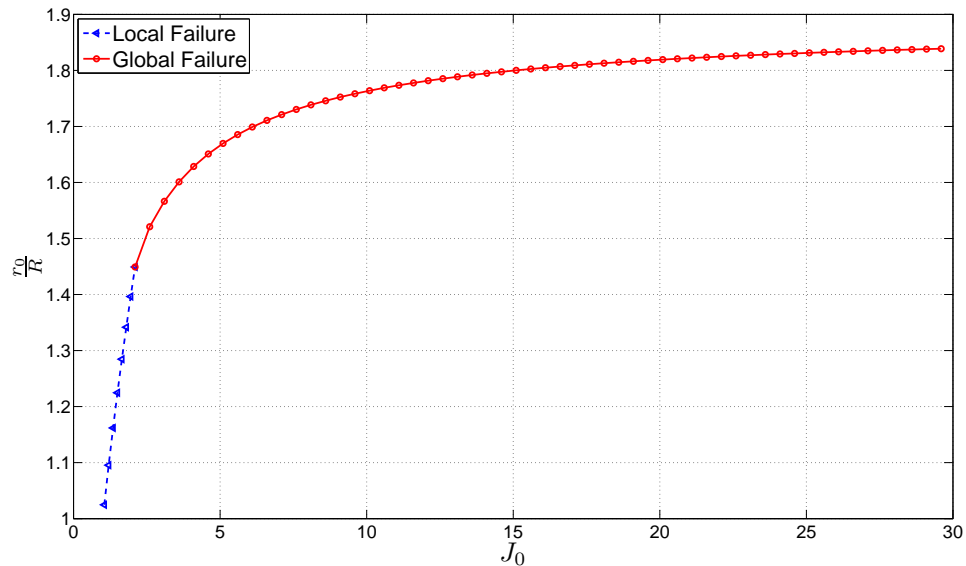
Figure 4.16: Critical inflation for cavitation ($\bar{\rho} \to 0$) for different values of J_0 where failure occurs immediately

4.0.5   Failure Displacement versus Inflation

The most interesting results of this project which reveal the critical effect of the non-dimensional radius of the indenter are shown in Figures 4.17, 4.18, 4.19 and 4.20. These figures show that for given values of J_0, $\bar{\rho}$ and r_0, what is the non-dimensional indenter displacement at which failure occurs and also they indicate the corresponding mode of failure. Therefore, the horizontal axis shows the non-dimensional inflation and the vertical axis shows the corresponding non-dimensional indenter displacement to reach to failure. These figures are prepared for the following values

$$J_0 = \{2, 5, 10, 15\}, \tag{4.18}$$
$$\bar{\rho} = \{0.01, 0.1, 0.2, 0.5, 1\}. \tag{4.19}$$

Each curve stops in the left end (lower inflation values) whenever the indenter reaches to the flat support ($\frac{d}{2r_0} = 1$) or wrinkling is observed which is the reason why some of the curves do not reach to the value $\frac{d}{2r_0} = 1$.

These figures show that for fixed inflation as the non-dimensional indenter size gets larger, the failure occurs at larger indenter displacements. Moreover, the curves are dominated by the local failure criteria when the indenter is small and as $\bar{\rho}$ increases, the role of the energy failure criteria becomes more evident such that at $\bar{\rho} = 1$, almost the entire graph is dominated by the global mode of failure due to energy. An exception for this observation is for the case $J_0 = 2$ at which global failure criteria plays no role and local mode of failure determines the entire graph.
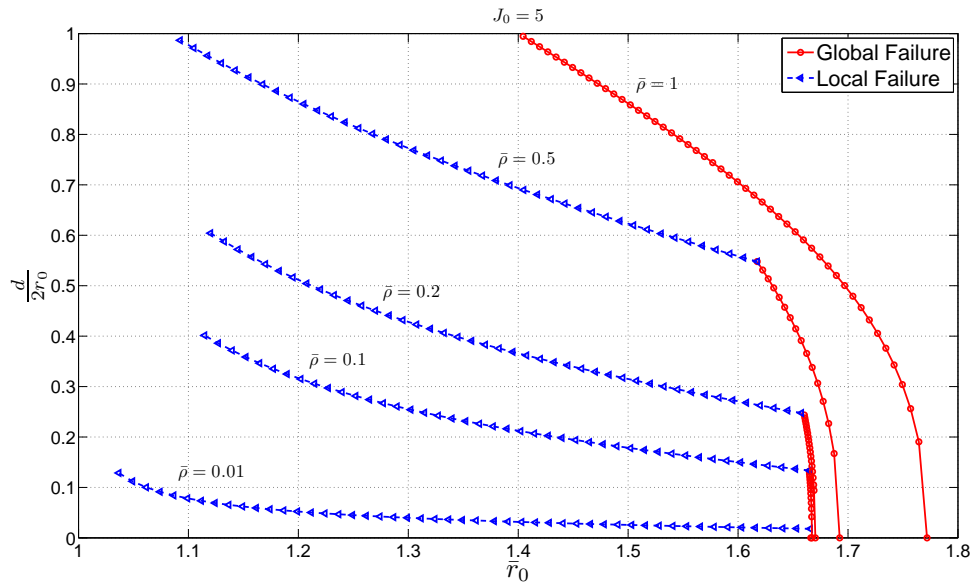
Figure 4.17: Failure displacement as a function of inflation for $J_0 = 5$
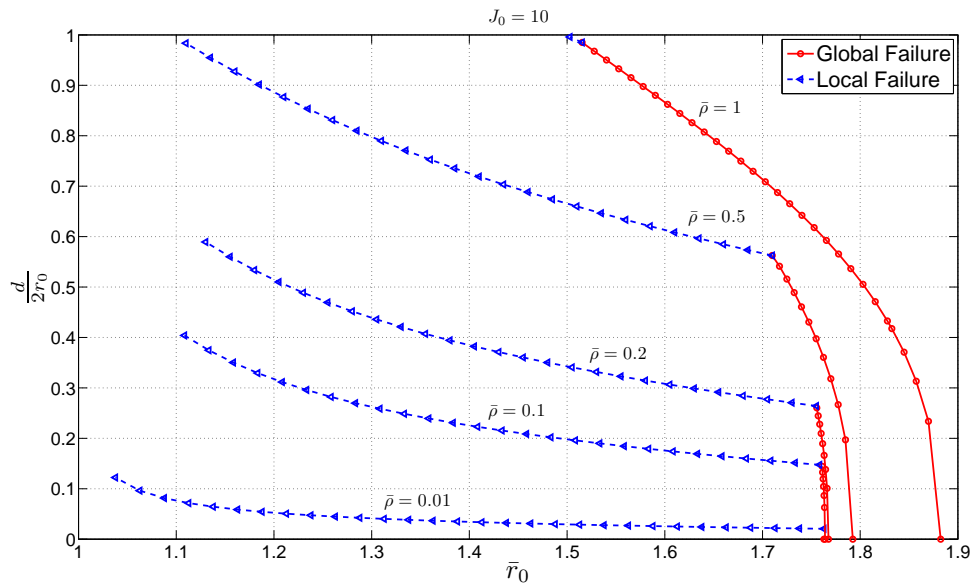
Figure 4.18: Failure displacement as a function of inflation for $J_0 = 10$
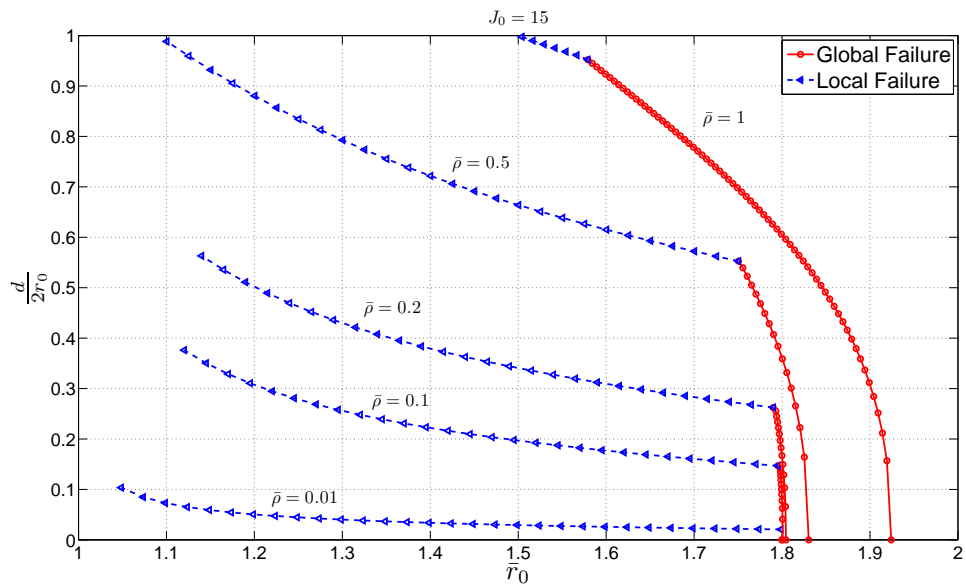
Figure 4.19: Failure displacement as a function of inflation for $J_0 = 15$
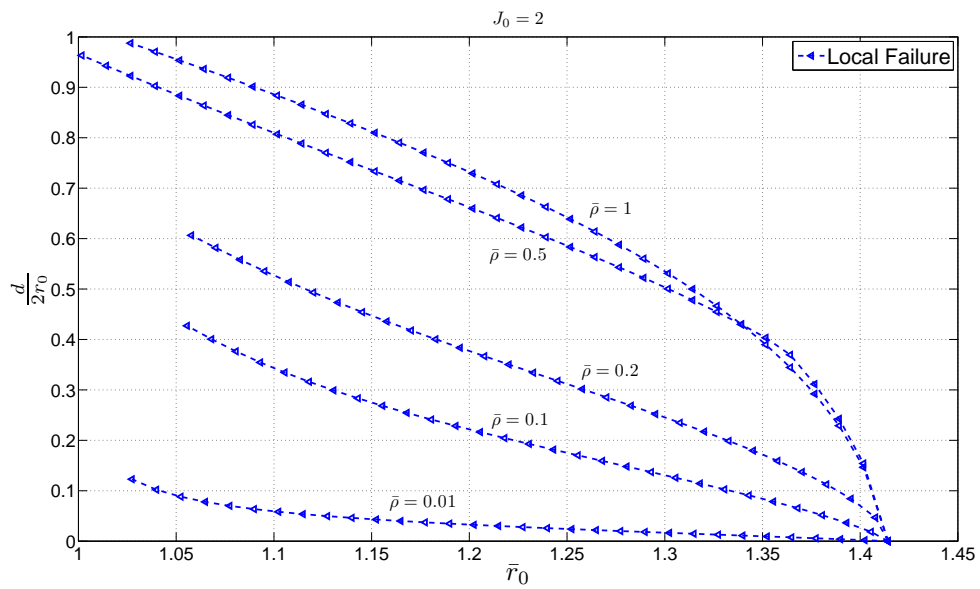
Figure 4.20: Failure displacement as a function of inflation for $J_0 = 2$

Chapter 5

Conclusions and Recommendations

In this thesis, we tried to model the indentation, penetration and cavitation of a spherical elastic membrane containing incompressible fluid using elastic approach. This work can provide more insight in the phenomenon of cavitation for a spherical membrane and its methods and findings can be extended to model realistic and practical problems such as cell microinjection.

We considered the possibility of cavitation in section 2.5. If the membrane could sustain pure cavitation, after penetration occurs we would continue to get more equilibrium solutions until we reach to the cavitated state in which a central traction free hole is formed around the indenter and only its edges are in contact with the indenter. However, the analysis showed in section 2.5 that when the penetration occurs, the membrane cannot keep the fluid inside and there is only one equilibrium solution after penetration and cavitation is the limit as $\bar{\rho} \to 0$.

A strain energy that can support penetration is presented in Section 2.2. In section 2.6, we used this strain energy function to compute the energy of the membrane at the penetrated state and to establish a critical value for the energy of the membrane beyond which the punctured membrane is energetically preferred. The analysis showed that this particular strain energy function gives a finite value for the energy of the penetrated state in this work as shown in equations 2.227, 2.228, 2.229 and 2.230; thus, it is able to model the penetration of the spherical membrane studied in this work. The analysis showed that this penetrated energy is a function of shear modulus of the membrane, the constant J_0 as well as the non-dimensional size of the indenter where the shear modulus is only scaling factor. It is interesting to note that the relative size of the indenter to the referential radius of the membrane plays an important role instead of the size of the indenter itself for analysis of the penetrated

state. Moreover, we found a requirement for the allowable non-dimensional size of the indenter for which the membrane can sustain penetration which is given in equation 2.232.

The computed penetrated energy is shown in figure 2.8 and the graph shows that the penetrated energy increases with the non-dimensional size of the indenter and decreases with J_0. This result is not surprising since for larger indenter, more deformation is required at the penetrated state which translates into more energy. Additionally, as J_0 increases, the material becomes less stiff thus it has less energy at the penetrated state. The fact that increase in J_0 makes the material less stiff is also verified by figure 4.9 which shows the indentation force. Furthermore, we showed that at the limit when the non-dimensional size of the indenter goes to zero, the penetrated energy approaches to a value given in equation 2.233 which is independent of J_0. This value represents the spontaneous cavitation. Moreover, this limit value represents the finite energy stored at a referential configuration of the membrane similar to the one shown in figure 2.1 but contains an infinitesimal cavity (micro-void) at the top pole. Based on this observation, for future work one can use this value to consider indentation and penetration of a spherical membrane containing a micro void[1] and to interpret the phenomenon of penetration for this spherical membrane as the growth of a pre-existing hole which is also suggested in [5] and [6].

As stated in section 2.7, we established a global failure criteria based on the finite energy of the penetrated state of the membrane. This mode of failure states that during the indentation, once the stored energy of the intact membrane exceeds the penetrated energy, the punctured state is energetically preferred and penetration occurs. Furthermore, we identified an additional local mode of failure that occurs when the local dilation at any point exceeds J_0 and the requirements of elastic material given in 2.90 are violated. These requirements stem from the convexity conditions and once they are violated, the material is no longer suitable for elasticity. Moreover, in numerical solutions for the cases we considered, it was observed that the point at which the local failure criteria occurs is the point directly under the tip of the indenter.

The influence of the non-dimensional size of the indenter for the dominance of each mode of failure manifests itself in figures 4.17, 4.18 and 4.19. According to these figures, for fixed inflation as the indenter gets larger, more indenter displacement is

---

[1]The fundamental difference will be the fact that the referential energy of the membrane is given by equation 2.233 rather than being zero.

required to reach to failure. Moreover, we observe that for small non-dimensional indenter size the dominant mode of failure is the local failure criteria and as the indenter gets larger, the effect of the global mode of failure becomes more pronounced. An exception for this observation happens when J_0 is relatively small[2] which is shown in figure 4.20 and the entire graph is dominated by the local failure criteria. We also considered a case for which the membrane is permeable such that the fluid pressure stays constant. Figures 4.14 and 4.15 show that in this case, the local failure criteria determined the failure point for the few examples that we considered and no failure due to energy was observed.

As another recommendation for future work, one can try to derive a different strain energy function that satisfies all the requirements mentioned in section 2.2 and observe how the change of strain energy function impacts the findings and conclusions of this work. We observed that finding a new strain energy function is challenging and it was not possible to formulate a different strain energy function in the limited time of this work. We speculate that if one finds a new strain energy function that can sustain penetration in the context of this work, the final form of that function will probably be more complicated and involves more terms than the one given in equation 2.117.

---

[2]Close to $J_0 = 2$.

Appendix A

Additional Results

In this chapter, extra indentation figures are presented.
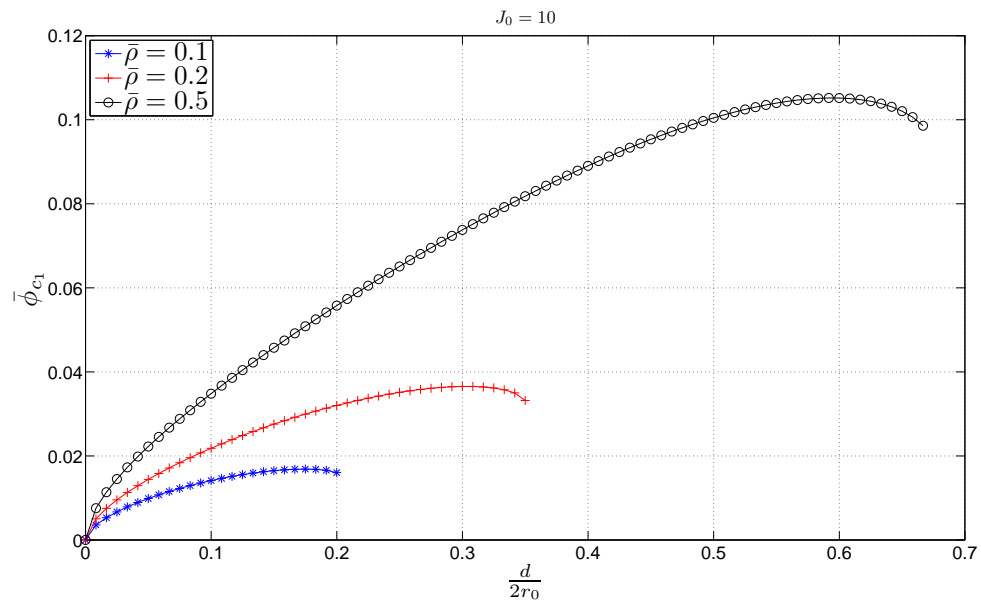
Figure A.1: $\bar{\phi}_{c_1}$ as a function of non-dimensional displacement for $J_0 = 10$
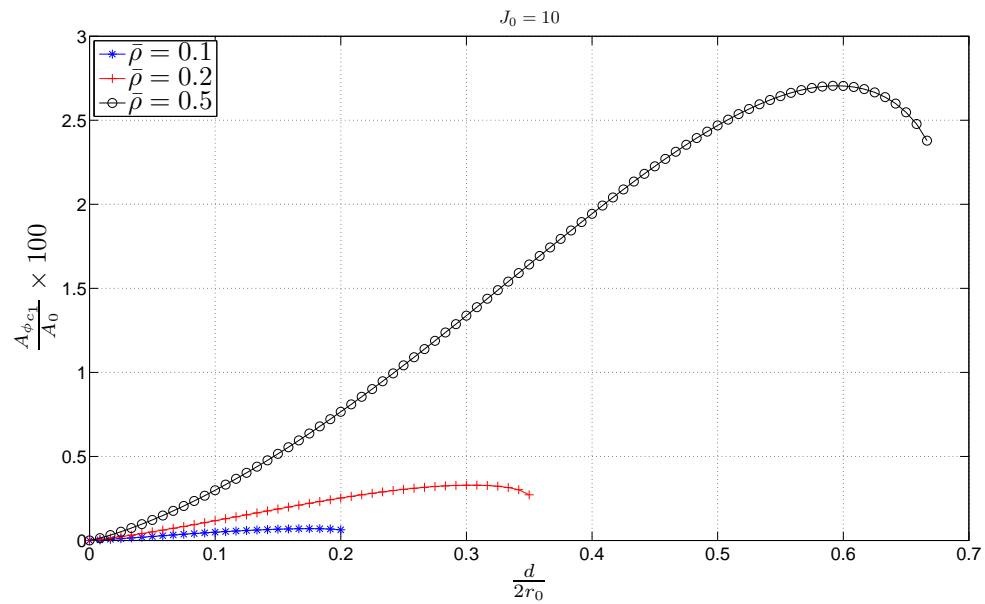
Figure A.2: $\frac{A_{\phi_{c_1}}}{A_0} \times 100$ as a function of non-dimensional displacement for $J_0 = 10$
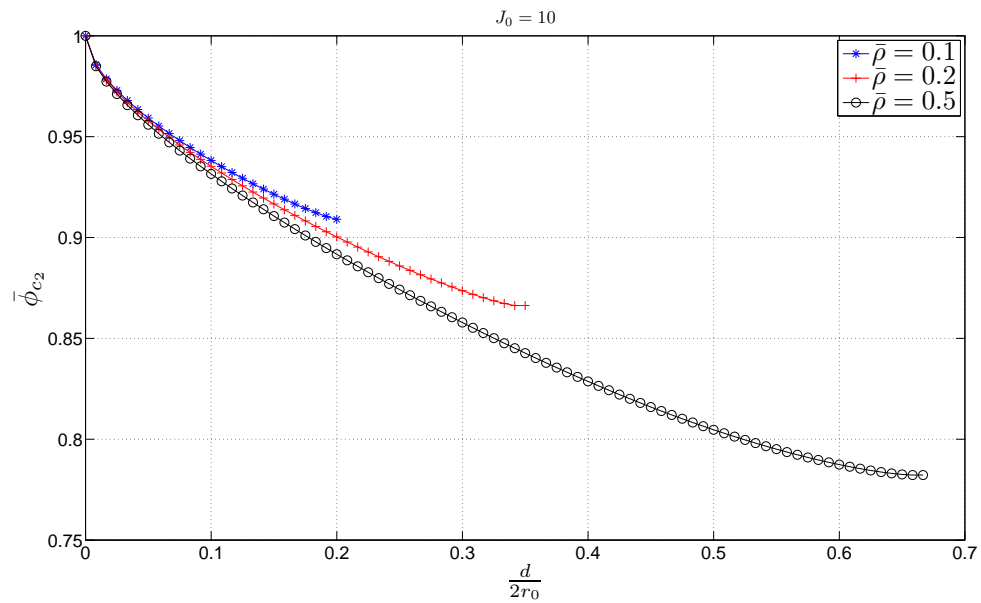
Figure A.3: $\bar{\phi}_{c_2}$ as a function of non-dimensional displacement for $J_0 = 10$
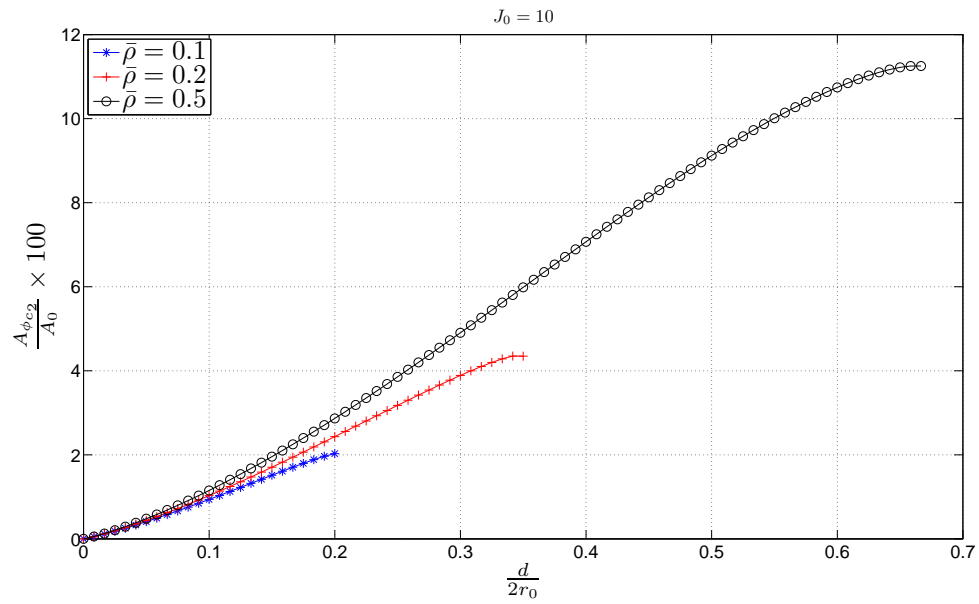
Figure A.4: $\frac{A_{\phi c_2}}{A_0} \times 100$ as a function of non-dimensional displacement for $J_0 = 10$
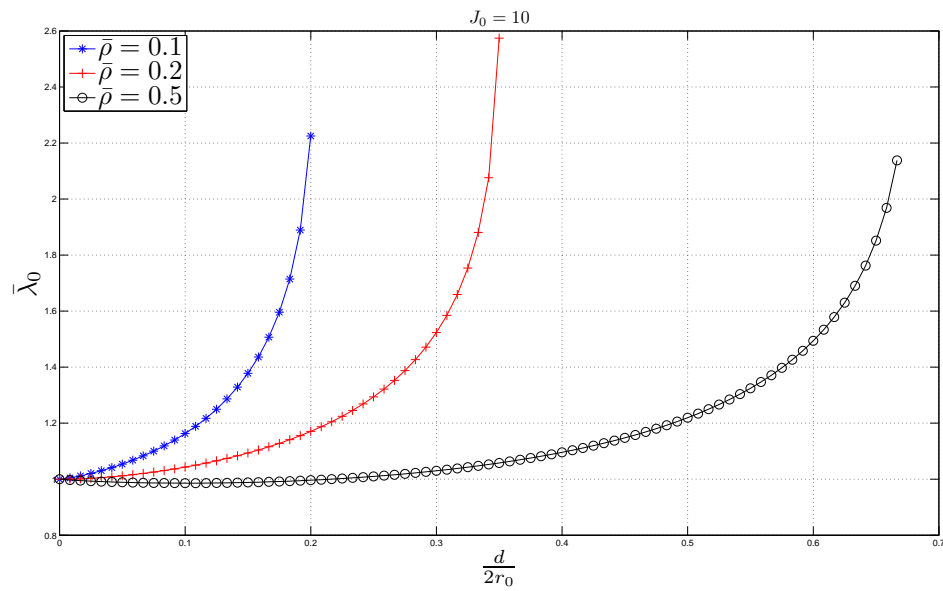
Figure A.5: $\bar{\lambda}_0$ as a function of non-dimensional displacement for $J_0 = 10$
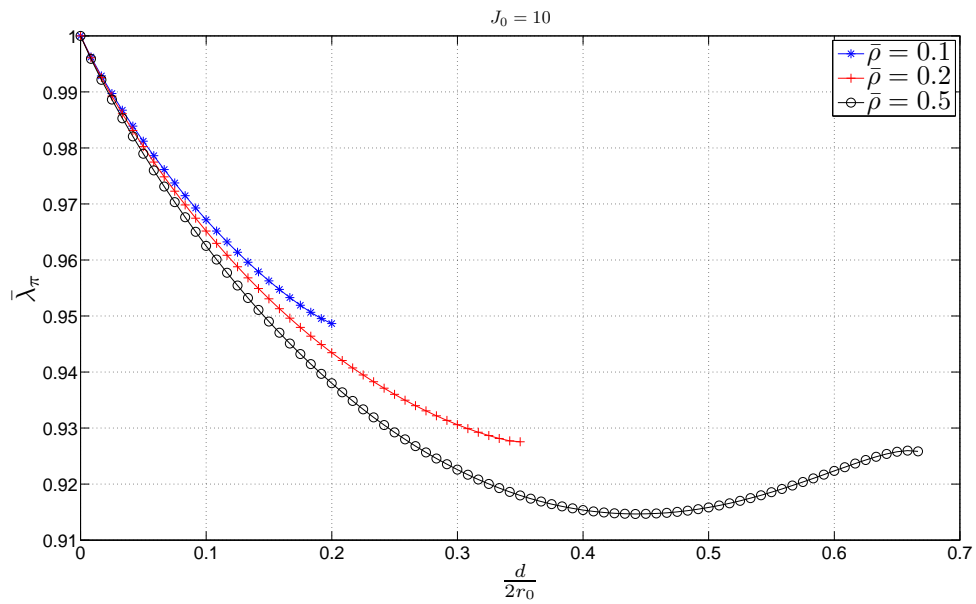
Figure A.6: $\bar{\lambda}_\pi$ as a function of non-dimensional displacement for $J_0 = 10$
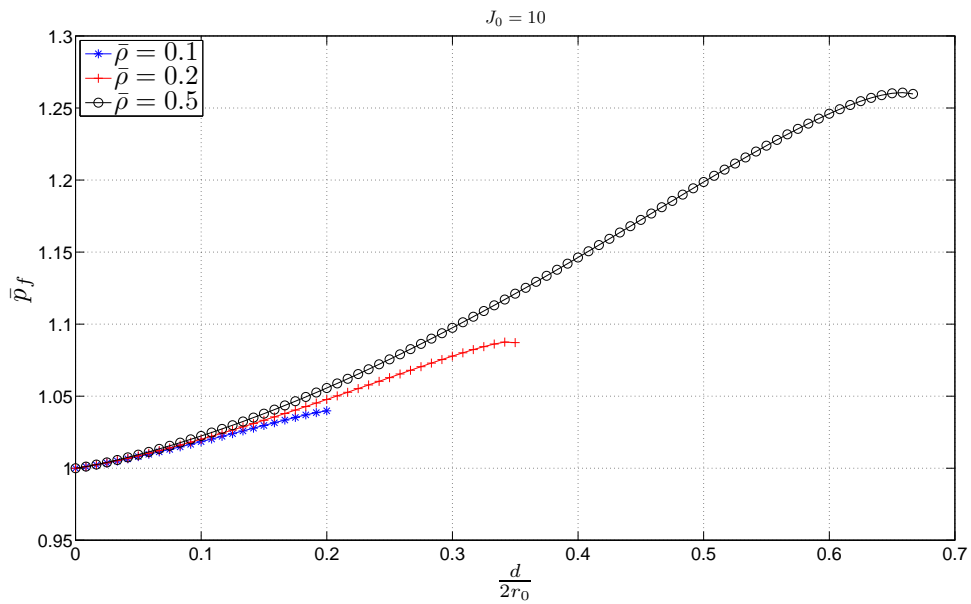
Figure A.7: $\bar{p}_f$ as a function of non-dimensional displacement for $J_0 = 10$
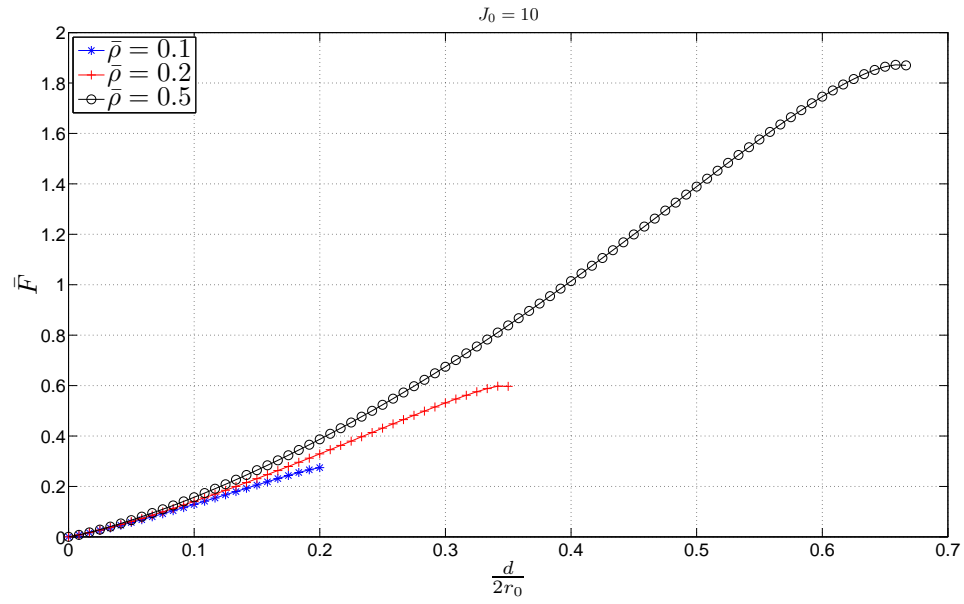
Figure A.8: $\bar{F}$ as a function of non-dimensional displacement for $J_0 = 10$
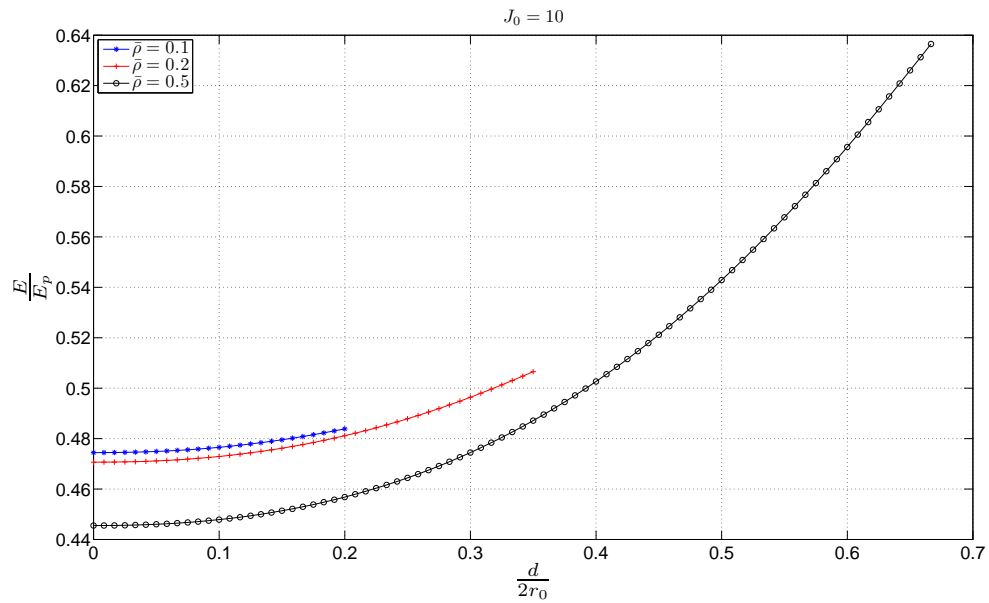
Figure A.9: Energy ratio $(\frac{E}{E_p})$ as a function of non-dimensional displacement for $J_0 = 10$
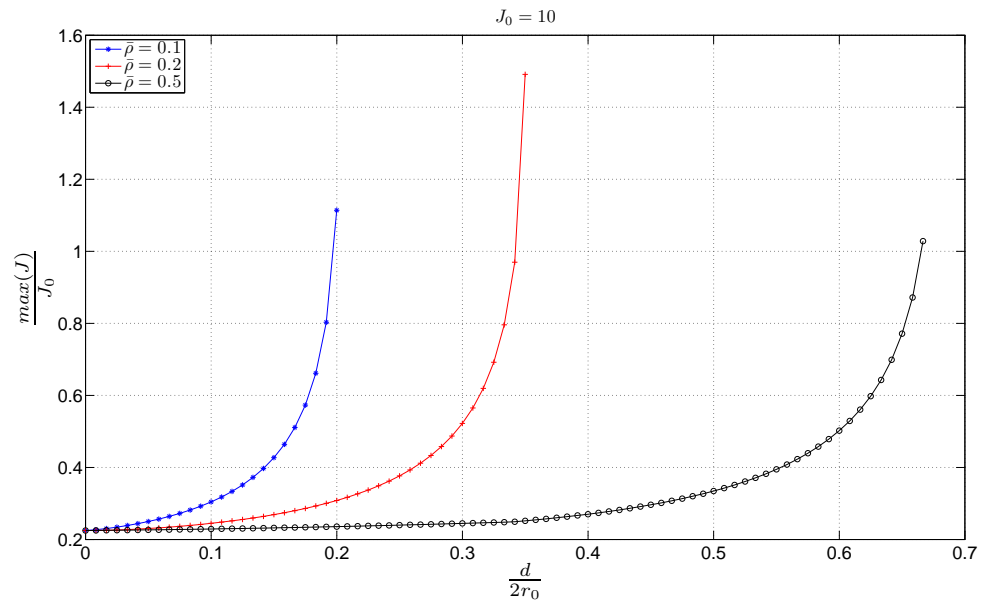
Figure A.10: Dilation ratio $(\frac{max(J)}{J_0})$ as a function of non-dimensional displacement for $J_0 = 10$

Bibliography

[1] J. M. Ball, "Discontinuous equilibrium solutions and cavitation in nonlinear elasticity," *Philosophical Transactions of the Royal Society of London. Series A, Mathematical and Physical Sciences*, vol. 306, No. 1496, pp. 557–611, 1982

[2] D. M. Haughton, "On non-existence of cavitation in incompressible elastic membranes," *The Quarterly Journal of Mechanics and Applied Mathematics*, vol. 39, pp. 289–296, 1986

[3] D. M. Haughton, "Cavitation in compressible elastic membranes," *International Journal of Engineering Science*, vol. 28, No. 2, pp. 163–168, 1990

[4] D.J. Steigmann, "Cavitation in elastic membranes - an example," *J. Elasticity*, vol. 28, pp. 277–287, 1992

[5] C. O. Horgan, R. Abeyaratne, "A bifurcation problem for a compressible nonlinearly elastic medium: growth of a micro-void," *Journal of Elasticity*, vol. 16, pp. 189–200, 1986

[6] D.J. Steigmann, "Puncturing a thin elastic sheet," *J. Non-Linear Mechanics*, vol. 40, pp. 255–270, 2005

[7] B. Nadler, D.J. Steigmann, "Modeling the indentation, penetration and cavitation of elastic membranes," *J. Mechanics and Physics of Solids*, vol. 54, pp. 2005–2029, 2006

[8] A.C. Pipkin, "The relaxed energy density for isotropic elastic membranes," *IMA Journal of Applied Mathematics*, vol. 36, pp. 85–99, 1986

[9] D.J. Steigmann, "Tension-field theory," *IMA Proceedings of the Royal Society of London*, vol. A 429, pp. 141–173, 1990

[10] A.C. Pipkin, "Convexity conditions for strain-dependent energy functions for membranes," *Archive for Rational Mechanics and Analysis*, vol. 121, pp. 361–376, 1993

[11] W. W. Feng, P. Huang, "On the general contact problem of an inflated nonlinear plane membrane," *International Journal of Solids and Structures*, vol. 11, pp. 437–448, 1975

[12] D. M. Haughton, "Axisymmetric elastic membranes subjected to fluid loading ," *IMA Journal of Applied Mathematics*, vol. 56, pp. 303–320, 1996

[13] X. Li, D. J. Steigmann, "Point loads on a hemispherical elastic membrane ," *International Journal of Non-Linear Mechanics*, vol. 30, No. 4, pp. 569–581, 1995

[14] D. J. Steigmann, "A simple model of the Treloar Kearsley instability ," *Mathematics and Mechanics of Solids*, vol. 12, No. 6, pp. 611–622, 2007

[15] B. Nadler, "On the contact of a spherical membrane enclosing a fluid with rigid parallel planes," *J. Non-Linear Mechanics*, vol. 45, pp. 294–300, 2010

[16] N. Kumar, A. DasGupta, "On the contact problem of an inflated spherical hyperelastic membrane," *J. Non-Linear Mechanics*, vol. 57, pp. 130–139, 2013

[17] A. Libai, D. Givoli, "Analysis of pulled axisymmetric membranes with wrinkling ," *International Journal of Solids and Structures*, vol. 39, pp. 1259–1274, 2002

[18] B. Nadler, T. Tang, "Decohesion of a rigid punch from non-linear membrane undergoing finite axisymmetric deformation ," *International Journal of Non-Linear Mechanics*, vol. 43, pp. 716–721, 2008

[19] C. T. Nguyen, T. Vu-Khanh, P. I. Dolez, J. Lara, "Puncture of elastomer membranes by medical needles. Part I: Mechanisms ," *International Journal of Fracture*, vol. 155, pp. 75–81, 2009

[20] T. Sohail, B. Nadler, "On the contact of an inflated spherical membrane fluid structure with a rigid conical indenter ," *Acta Mechanica*, vol. 218, pp. 225–235, 2011

[21] Ciarlet, PG 2005, An introduction to differential geometry with applications to elasticity, Springer, Netherlands

[22] Eringen, A.C. [1967], Mechanics of Continua, John Wiley and Sons Ltd., USA

[23] H. Andra, M. K. Warby, J. R. Whiteman, "Contact problems of hyperelastic membranes: existence theory ," *Mathematical Methods in the Applied Sciences*, vol. 23, pp. 865–895, 2000

[24] M. R. Begley, T. J. Mackin, "Spherical indentation of freestanding circular thin films in the membrane regime ," *Journal of the Mechanics and Physics of Solids*, vol. 52, pp. 2005–2023, 2004

[25] S. P. Pearce, J. R. King, M. J. Holdsworth, "Axisymmetric indentation of curved elastic membranes by a convex rigid indenter," *International Journal of Non-Linear Mechanics*, vol. 46, pp. 1128–1138, 2011

[26] Gurtin, M.E. [2003], An Introduction to Continuum Mechanics, ELSEVIER, Kundli

[27] Holzapfel, G.A. [2000], Non linear Solid Mechanics, John Wiley and Sons Ltd., England

[28] Wriggers, P. [2008], Nonlinear Finite Element Methods, Springer-Verlag, Berlin

[29] Truesdell, C., and Noll, W. [2004], The Non-Linear Field Theories of Mechanics, 3rd edn., Springer-Verlag, Berlin